University of South-Eastern Norway

Faculty of Technology, Natural Sciences and Maritime Sciences

Master's Thesis

Final Project / JMN500

2024 *Spring*

Ulzhan Bassembek / candidate number 8001

Electrode optimisation towards lowering self-discharge of carbon nanotubes-based supercapacitors

in collaboration with nanoCaps company

Supervisors:
Pr. Pai Lu, Pr. Per Øhlckers, Dr. Eivind Bardalen

University of South-Eastern Norway
Faculty of Technology, Natural Sciences and Maritime Sciences
Institute of Microsystems
PO Box 4
3199 Borre

http://www.usn.no

This thesis is worth 30 study points

Abstract

Currently tremendous work is done to improve capacitance of supercapacitors. However, such important supercapacitor parameter as self-discharge is often overlooked, being a bottleneck issue in energy storage applications of supercapacitors. It requires more study and concrete methods to supress self-discharge of supercapacitors.

In this study self-discharge of carbon nanotubes-based supercapacitors is studied. Hydrogen and nitrogen annealing heat treatment is introduced a method of self-discharge improvement. Moreover, an optimal recipe of the annealing procedure is determined with temperature of 500°C, duration of 30 minutes and H_2:N_2 gas composition of 20 sccm: 200 sccm.

It is shown that for CNT-based supercapacitors with capacitance in the range of 20 mF the self-discharge has been improved by 62.3% by implementing introduced annealing heat treatment. In addition, FE-SEM, EDX and XRD sample characterisation has been performed to analyse the difference in electrodes before and after annealing.

Moreover, the studied annealed electrodes-based supercapacitors showed 6.6% better self-discharge performance than a commercial capacitor.

Furthermore, after consideration of challenges and limitations, certain methods to suppress self-discharge of CNT based supercapacitors even further are suggested for future work, including closer investigation of annealing parameters and usage of gold-plated coin cell cases for coin cell assembly.

Keywords: *supercapacitors, carbon nanotubes, self-discharge, annealing, heat treatment*

Table of contents

Foreword

The author would like to thank Pr. Pai Lu, Pr. Per Øhlckers and Dr. Eivind Bardalen for their guidance and support thought the thesis work. The author is grateful for support and assistance from nanoCaps colleagues, lab engineers and all people who helped in one way or another.

This work is performed as a part of Smart Systems Integrated Solutions Joint Master Degree Program. The project is done in collaboration with nanoCaps company.

OriginPro and Microsoft Excel software have been used for calculations and data representation. Microsoft Office software has been used to type the thesis.

Borre, Norway / 30.06.2024

Ulzhan Bassembek

1. Introduction

1.1 Motivation

With accelerated development of energy market, especially renewables, electrochemical capacitors can be considered for energy storage, which means not only capacitance, but also self-discharge plays a key role in the device performance. The purpose of the project is to lower self-discharge of carbon nanotubes-based supercapacitors, thus improving their performance. This is done with hydrogen (H_2) and nitrogen (N_2) annealing. The main aim is to identify optimal parameters of the H_2 + N_2 annealing, such as temperature, annealing duration and H_2:N_2 gas composition in terms of gas flow rates.

1.2 Theoretical background

In this section the principles behind carbon nanotubes-based supercapacitors are explained.

1.2.1 Carbon nanotubes

Carbon nanotubes are tubular structures of carbon atoms, where the latest are arranged in honeycomb way. Every carbon is bonded to three neighboring carbon atoms through sp^2 hybridization, forming a seamless shell. CNTs can be considered as tubular micro-crystals of graphite.
As implies from their name, carbon nanotubes have a diameter in nanoscale and significantly larger length. Having high length-to-diameter ratio, CNTs are considered as quazi one dimensional structures.

CNTs can be represented as a large strip of graphene or graphite for multi-layered CNTS sheet wrapped up [1] as shown in Figure 1. There are two types of CNTs in terms of number of layers of graphene sheets, there are single-walled carbon

nanotubes (SWCNT) and multi-walled carbon nanotubes (MWCNT), sometimes double-walled carbon nanotubes are differentiated as one more type [2],[3].

Moreover, CNTs can show different conductivity properties, i.e. they are metallic and semiconductor CNTs. Namely, SWCNTs can possess both metallic or semiconducting properties, which depends on the diameter and chiral angles. Metallic SWCNTs (m-SWCNTs) have zero band gap between conduction and valence band. In contrast, semiconducting SWCNTs (s-SWCNTs) have a non-zero energy gap. As for MWCNTs, they are considered metallic [2].

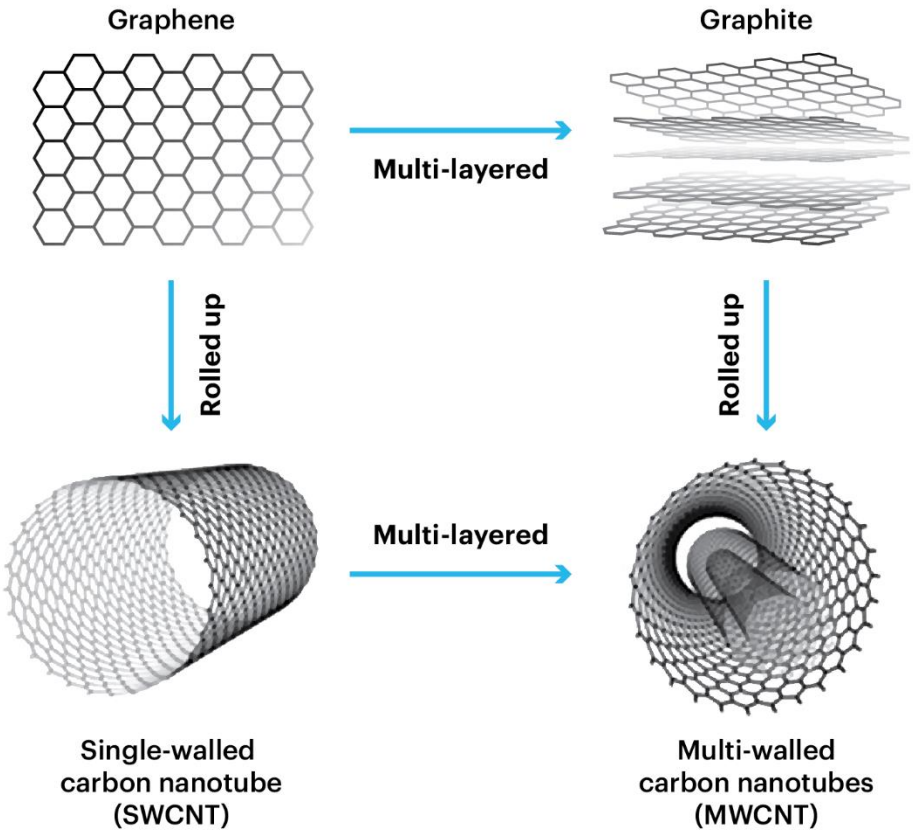

Figure 1. Carbon nanotube types: single-walled and multi-walled CNTs [4]

CNT are one of the common electrode materials for supercapacitors, that have such advantage over porous carbon material (e.g. polymer derived carbon, chemical/physical activated carbon etc) as their high electrical conductivity, leading to fast charge transferring [5], [6], [7].

1.2.2 CNT growth

One of the commonly used CNT growth mechanisms is chemical vapour deposition (CVD)[8], [9]. In this study carbon nanotubes grown under atmospheric pressure CVD are considered, implying that APCVD is applied.

The principle of CVD based carbon nanotubes growth is in decomposition of hydrocarbon such as methane, ethylene or acetylene or into carbon, followed by growth of CNT on catalyst particle on substrates. Metal-based nanoparticles such as nickel, cobalt or iron nanoparticles commonly act as catalysts in CVD growth, their sizes influence the diameter of CNTs [10].

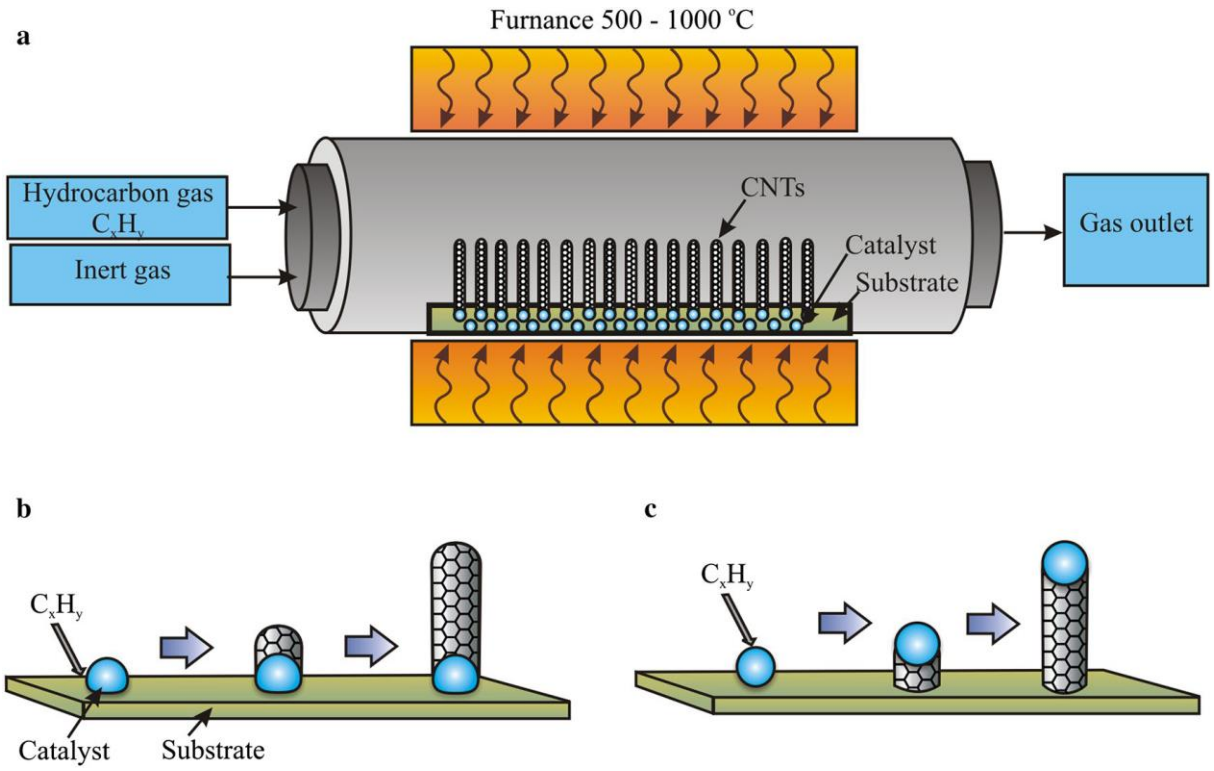

Figure 2. Chemical vapor deposition (CVD) process: ***a*** *CNT synthesis in CVD reactor;* ***b*** *basegrowth mechanism of CNT;* ***c*** *tipgrowth mechanism of CNT* [10]

CVD synthesis process shown in occurs in reactors consisting of a reaction chamber and quartz tubes, through which inert gas and hydrocarbon are introduced. A substrate is heated to 550 - 700°C. Due to thermal decomposition of hydrocarbons carbon is formed. When carbon concentration reaches certain threshold, it starts to form a semi

fullerene (pentagonal base) cap, acting as a foundation for the growth of a cylindrical shell carbon nanotube. Given a continuous formation of carbon from the hydrocarbon source, carbon nanotubes continue to grow [10]. This is followed by a so-called reduction process, which is removing of catalyst nanoparticle from the samples by introducing hydrogen gas.

CVD based carbon nanotubes growth can be suitable for industry-scale production due to comparably simple equipment and mild temperature and pressure conditions [10].

Concerning industry application, there are numerous fields where carbon nanotubes can be effectively used due to their unique mechanical, thermal and electrochemical properties [11], [12]. As their strong Van der Waak force interaction between CNTs [13], CNT based material possess high strength and can be used enhancing of materials, such as high-performance composites [14]. High electronic transport capability of CNTs make them potential source of nanowires[13]. Moreover, metallic CNTs can be applied as a material for the source/drain electrodes for organic field-effect-transistors (OFETs). Semiconductor SWCNT can be potential active material for field-effect-transistors FETs) [13].

1.2.3 CNT based supercapacitors

One of the most common applications of CNTs is electrochemical double layer capacitors (EDLC), where electrodes are CNT based [15],[16],[17] . In these capacitors, a voltage applied between electrodes immersed in electrolyte cause formation of charged double layer [18], where energy is stored as shown in Figure 3.

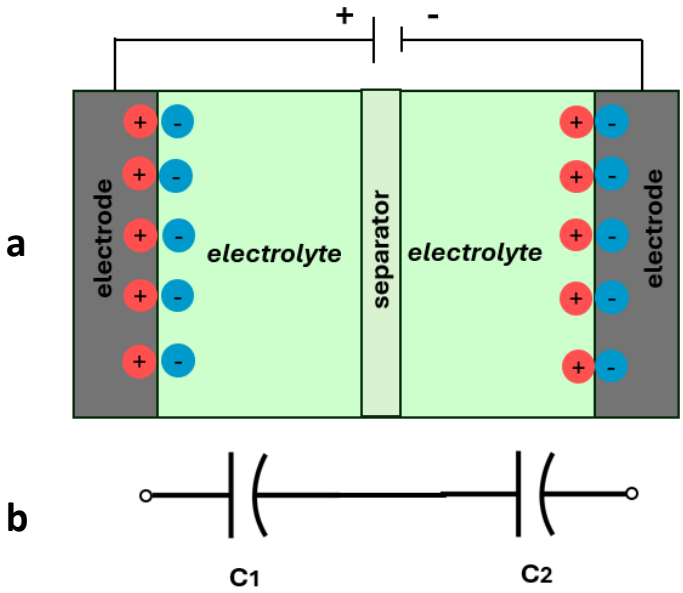

Figure 3. Electric double layer capacitor (EDLC):
a. Schematic representation; b. Equivalent electrode capacitances

The capacitance of EDLCs is highly dependent on the active surface area of the electrodes. Using CNTs for electrodes significantly increases electrode surface area [13], leading to extremely high capacitance, implying supercapacitance, where ‘supercapacitor’ term takes its origin from.

1.2.4 Mechanism of self-discharge

Besides capacitance, self-discharge is one of the main parameters of supercapacitors. The mechanism of self-discharge phenomenon can be subdivided into three principles: ohmic leakage, parasitic faradaic reaction and charge redistribution [19], [20], [21].

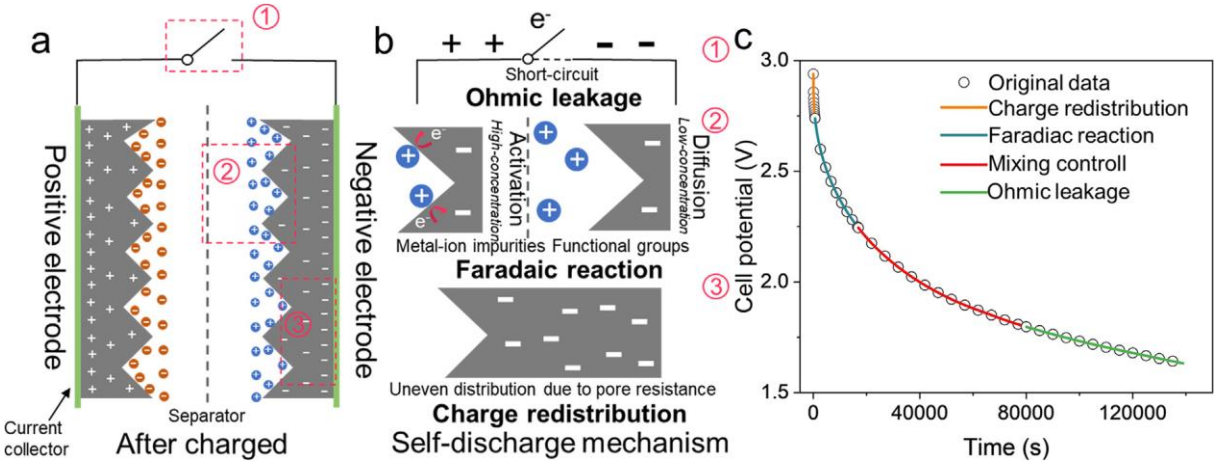

Figure 4. Self-discharge mechanism of a supercapacitor: a. A supercapacitor after being charge, b. Types of self-discharge mechanism, c. A voltage decay curve considering three type of self-discharge mechanism [19]

Ohmic leakage is caused by the resistive pathway between the positive and negative electrodes. Voltage can be expressed as follows:

$$V = V_0 \, exp\left(-\frac{t}{RC}\right) \qquad \textit{(Equation 1)}$$

where V_0 is the initial voltage, t is delay time, RC is time constant. From this formula, it can be concluded that self-discharge depends on resistance of ohmic leakage and capacitance of a supercapacitor. Self-discharge caused ohmic leakage can be a result of possible internal short circuit. In this type of self-discharge, there is only charge transfer, and no chemical reactions are involved [19].

Parasitic faradaic reaction is oxidation or reduction of species on electrode surface, due to which charge balance between electrode and electrolyte can result in energy loss [19]. Parasitic faradaic reaction in its turn can be subdivided into two reactions: activation-controlled and diffusion-controlled [19].

The activation-controlled reaction is caused by presence of relatively high concentration of impurities in the electrode or electrolyte, such that ions in the pores of the electrode can exchange electrons with electrode charge. During this process a potential-dependent Faraday charge-transfer reaction takes place in the double layer. The activation-controlled reaction can also be caused by the overcharge of a supercapacitor, i.e. when a supercapacitor charge is higher than the electrolyte decomposition potential limit. The voltage decay during activation-controlled Faraday reaction can be determined as follows

$$V = -\frac{RT}{\alpha F} ln \frac{\alpha F_{i_0}}{RTC} - \frac{RT}{\alpha F} ln\,(t + \frac{C\tau}{i_0}) \qquad \textit{(Equation 2)}$$

where R is gas constant, T is temperature, α is transfer coefficient, F is Faraday constant, i_0 is exchange current density, C is interfacial capacitance, and τ is integration constant [19].

As for diffusion-controlled reaction, it occurs on the outer surface of electrodes, self-discharge does not happen on the inner surface of the pores. This is because under low concentration, reactant can be fully consumed in pores with high surface area/ volume ratio. In this case voltage decay can be determined as follows:

$$V = V_i - \frac{2zFAD^{\frac{1}{2}}c_0}{C} t^{\frac{1}{2}} \qquad \textit{(Equation 3)}$$

where V_i is initial voltage, z is charge, D is diffusion coefficient, c_0 is initial concentration and A is area of an electrode [19].

Charge redistribution is caused by unequal charge distribution during charging, which in its turn results in movement of charge barrier during voltage delay. For instance, for some porous electrode materials, electrode surface close to the current collector can charge quicker and can therefore reach the stated voltage faster than the area inside. Therefore, targeted charge for inner material cannot be ensured because voltage value is measured on the electrode surface. After charging, during delay, charged ions on electrode surface can gradually move inside, leading to measured voltage decrease. The charge redistribution can be subdivided into two types: diffusion-limited and resistance-limited. Diffusion-limited charge redistribution is caused by diffusion of charges close to or on electrode surface, whereas resistance-limited charge redistribution comes from resistance elements such as electronic/ionic resistance or solution resistance in pores [19].

Practically, these three parts of self-discharge mechanism occur simultaneously, resulting into complex self-discharge behaviour in real supercapacitors. Combining ohmic leakage, Faradaic diffusion and charge redistribution, real self-discharge mechanism of supercapacitors can be expressed as follows:

$$V = V_0\, exp\left(\frac{-t}{RC}\right) - Bt^{\frac{1}{2}} - m - nln\left(t + \frac{CK}{i_0}\right) \qquad \textit{(Equation 4)}$$

where B is Faradaic diffusion-related variable and m and n are Faradaic activation-related variables [19].

1.3 Research efforts on self-discharge decrease of CNT based supercapacitors

1.3.1 Asymmetric all-solid-state supercapacitors

Ovhal et al [22] introduced the fabrication of Asymmetric all-solid-state supercapacitors (ASSC) device with carbon cloth (CC)/nickel hydroxide (Ni(OH)2) and CC/CNTs electrodes as shown in Figure 5. These devices demonstrated an energy density of 132.7 Wh/kg. Regarding capacitance, novel groove-and-crest structure of CC/CNTs electrodes resulted in a capacitance of 278 mF/cm^2.

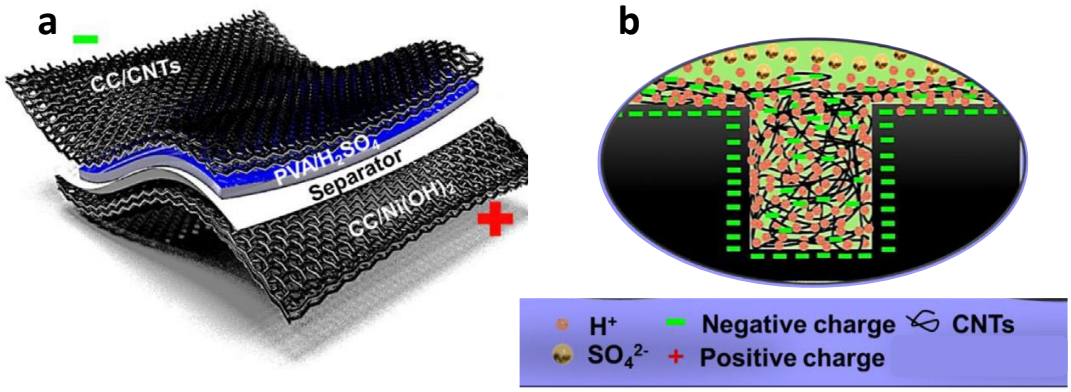

Figure 5. Asymmetric all-solid-state supercapacitor with CC/Ni(OH)2 and CC/CNTs electrode: a. A schematic of device structure, b. a schematic representation of self-discharging [22]

It was found out that self-discharge performance depends on such parameters as temperature, device voltage, current density and charge time [22], [23]. For ASSC device optimal charging time and current density were determined to be 30 min and 1.0 mA/cm^2, respectively. Groove-and-crest structure facilitated the improvement of capacitance and self-discharge behaviour. Self-discharge test results showed that 0.32 V potential was maintained after 166 minutes of initial 2.0 V charge, which means that 84% of initial charge has been lost.

1.3.2 CNT diameter size effect on self-discharge

Zhang et al [24] conducted a study on influence of multi walled carbon nanotubes (MWCNT) diameter of self-discharge of supercapacitors. MWCNTs with 20, 30, and 50 nm diameters have been considered to investigate pore-size effect on the self-discharge behaviour. Open circuit voltage decay measurements showed that among studied samples, CNTs with 20 nm diameter showed the lowest and CNTs with 50 nm the highest self-discharge rates. This implies that the self-discharge of the MWCNT supercapacitors can increase with the diameter of MWCNTs [24].

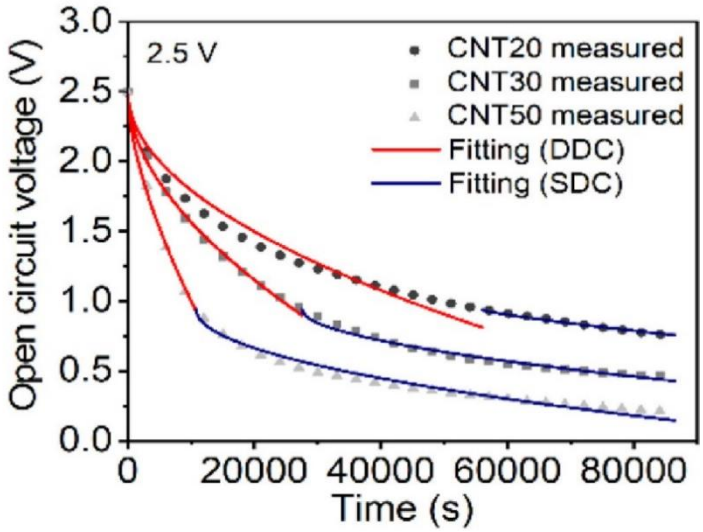

Figure 6. Self-discharge of carbon nanotubes with diameter of 20 nm, 30 nm and 50 nm, labelled as CNT20, CNT30 and CNT50 respectively. The supercapacitors were charged to 2.5 V. Self-discharge plots were fitted using divided diffusion-controlled (DDC) model illustrated in red and single diffusion-controlled (SDC) model illustrated in blue [24].

To study self-discharge behaviour in details, open circuit voltage had been fitted, considering ohmic leakage and diffusion-controlled faradaic processes, including both divided diffusion-controlled (DDC) and single diffusion-controlled (SDC) stage. It was concluded that diffusion parameters increased with the rise in CNT diameter, being correlated with their increase in self-discharge rates. This could be caused by quicker ion diffusion in electrodes with larger pore sizes [24].

From the graph it can be seen that 1.0 V potential was maintained after 60000 seconds (around 15 hours) out of initial 2.5 V charge, which means that 60% of initial charge has been lost.

1.3.3 Influence of functional groups presence on self-discharge

Zhang et al [25] investigated the effect of functional groups presence on self-discharge of single wall carbon nanotubes-based (SWNT) supercapacitors. SWNT electrodes had been produced by CVD process. The samples were referred as SWNT. To vary concentration of functional groups, post-treatment had been applied. To reduce functional group content SWNT samples were heat-treated at 400°C in argon environment had been applied, produce samples were referred as r-SWNT. In contrast, to increase the content of functional groups, the SWNT samples were soaked for 10 minutes in KMnO4 solution, namely 0.1 g KMnO4 in 20mLconcentrated sulfuric acid. After that the samples were rinsed with hydrochloric acid and copious distilled water. The obtained samples were referred as o-SWNT.

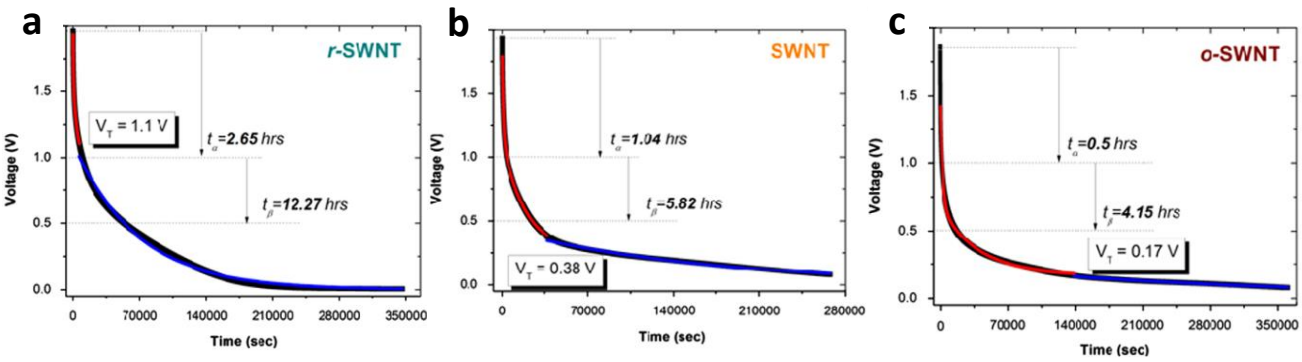

Figure 7. Self-discharge behaviour: a. r-SWNT samples, b. SWNT samples, c, o-SWNT. Self-discharge plot is depicted in black, DPD (divided potential driving model) fitted results in red and SPD (Single Potential Driving) model fitted results in blue [25].

From the self-discharge tests, it was concluded that SWNT samples with higher functional groups concentration had higher self-discharge rate. So, the best self-discharge result was from SWNT with reduced content of functional groups, having around 0.4 V at 70000 seconds, meaning that 80% of initial 2.0 V had been lost.

1.3.4 Conclusion on research on self-discharge improvement of CNT supercapacitors

Though tremendous work has been made to improve capacitance of supercapacitors, there is still limited research work done to lower self-discharge, especially of CNT based supercapacitors. Speaking about existing self-discharge suppress research efforts made (considered earlier), self-discharge from 60 to 84% can occurs even after improvement of CNT electrodes. The effective strategies for lowering the self-discharge are still limited. Therefore, more detailed study on self-discharge of CNT-based supercapacitors is needed with further improvement of self-discharge behaviour.

1.4 Research problem statement

Currently considerable advances in improvement of capacitance of CNT-based supercapacitors have been made, reaching capacitance of over several hundred farads per square centimetre. However, the self-discharge is another fundamental parameter of a supercapacitor, which can still be a bottleneck for the application of supercapacitors in some specific areas such as energy storage. For instance, currently over 90% of the initial charge is lost by using after around 14 hours of open circuit voltage decay at nanoCaps company.

There is still lack of research on self-discharge of supercapacitors overall, and of CNT-based supercapacitors in particular. Currently, there is a need to study lowering significantly self-discharge of CNT-based supercapacitors as manufacturers aim to suppress self-discharge parameter to advance in energy storage applications.

What is more, a concreate method and optimal recipe is needed to improve self-discharge performance of CNT electrodes. This can help to solve self-discharge bottleneck problem in industry level, including facilitating CNT-based supercapacitors manufacturing at nanoCaps company.

This project study aims to solve a problem of self-discharge of CNT-based supercapacitors and can facilitate in self-discharge research. This is done by introducing hydrogen and nitrogen annealing heat treatment of CNT electrodes. Moreover, an optimal recipe of the annealing treatment is to be determined, including optimal parameters (temperature, time and gases composition) for self-discharge lowering. Furthermore, the effect of hydrogen and nitrogen annealing on CNT based electrodes is to be studied performing samples characterisation and comparing samples before and after annealing.

2. Methods

2.1 Annealing

To improve a self-discharge performance of supercapacitors, in this study hydrogen and nitrogen annealing (H_2+N_2 annealing) is used. The annealing is performed in chemical vapor deposition chamber in a quartz tube under atmospheric pressure with introducing hydrogen (H_2) and nitrogen gases (N_2) as shown in Figure 8. The optimal annealing parameters, such as flow rates of the gases, annealing duration and temperature of heat treatment is to be determined as explained in the next section.

During CNT synthesis, oxygen from $NiSO_4$ solution can react with carbon and produce bonds of functional groups. For instance, such functional groups as C = O, –COOH and -COO have been detected on MWCNT electrode surface [24], [26], [27].

It is expected that introduced hydrogen will react with amorphous carbon and functional groups (i.e. C=O, -COO, -COOH) and remove them from the surface of the sample, thus leading to purification of CNT electrode surface. This in its turn can improve the self-discharge performance of supercapacitors made from the annealed electrodes [28].

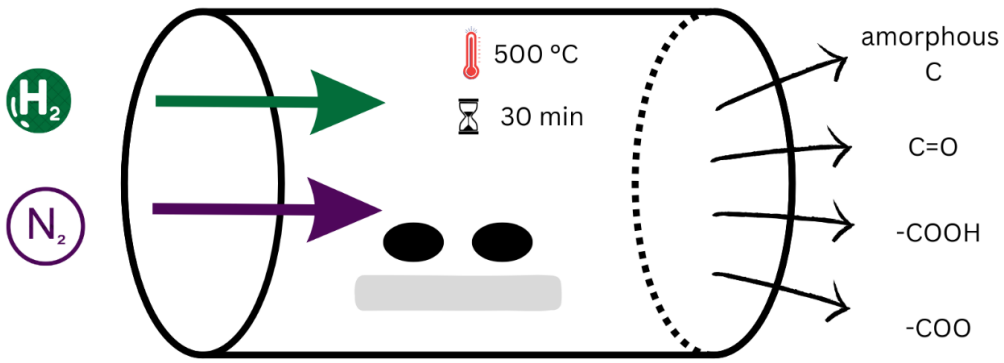

Figure 8. Schematics of the annealing process. An example of treatment under 500° C temperature and duration of 30 minutes.

2.2 Parameter optimisation

The main aim is to identify optimal parameters of the H_2 + N_2 annealing, such as temperature, duration, flow rate of H_2 and N_2 gases.

This is done by performing annealing under varying temperate, time and gases flow rate, as shown in Figure 9. For temperature, 5 values have been chosen ranging from 200°C to 600°C, for duration of annealing 5 values from 20 minutes to 60 minutes have been selected. For hydrogen flowrate 4 values have been considered, namely 20, 40, 50 and 100 standard cubic centimetres per minute (sccm), as for nitrogen gas, 2 values (500 sccm and 200 sccm) have been considered.

Figure 9. Annealed parameters used

As it can been seen from Figure 9, in this project four annealing parameters have been considered. The optimisation was started from altering temperature, since heating the CVD chamber up to certain temperature affected the duration of the whole process, including heating-up and cooling. It is important to note that one parameter was changed per experiment, meaning other three parameters were fixed. Once the temperature value which led to best self-discharge was determined, this temperature was fixed, and annealing time was altered next. After optimal annealing duration was

identified, hydrogen and nitrogen flowrates have been changed, leading to determining to final optimal recipe of annealing.

It is important to note that hydrogen and nitrogen gases are introduced at the stable flow rates throughout the whole annealing experiment, i.e. during heating-up to annealing temperature, annealing itself and natural cooling down, temperature profile of annealing experiment is shown in Graph 1. Before heating starts, nitrogen gas is introduced for 10 minutes, as a measure of purging and cleaning sample surface from possible contamination such as dust particles.

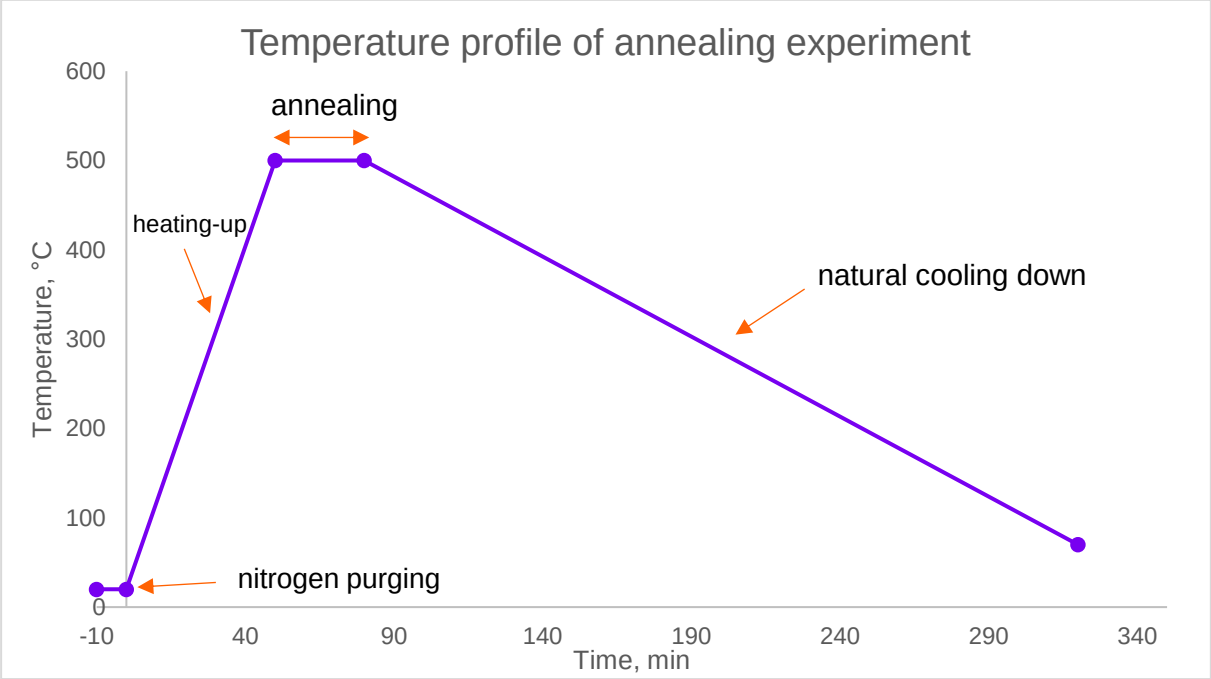

Graph 1. Temperature profile of annealing experiment, with example annealing temperature 500°C

3. Procedures

The methods have been implemented following the procedures: preparation of electrodes, annealing experiment, coin cell assembly, measurements and calculations, followed by sample characterisation as shown below.

3.1 Sample information

In this study a CNT sample has been provided by nanoCaps company. The aluminium foil thickness is 30 um. Nickel nanoparticles were introduced by spray coating nickel sulfate ($NiSO_4$) 30.8uL/cm2 on the substrate. Carbon nanotubes were grown by performing CVD under 580°C for 20 minutes, with introduction of argon (Ar), hydrogen (H_2) and acetylene (C_2H_2) gases with $Ar:H_2:C_2H_2$ gas composition of 400:1000:200 in sccm. These parameters are organised in
Table *1*.

Table 1. Information on CNT sample used in the study

Sample used (provided by nanoCaps)	**Ni particles deposition method**	**$Ar:H_2:C_2H_2$ gas composition in sccm**	**CVD temperature**	**CVD time**
A33	Spray coating of nickel sulphate with 30.8uL/cm2	400:1000:200	580°C	20 min

3.2 Preparation of electrodes

The electrodes of 14 mm diameter are cut out from the larger sample strip with a puncher or punching machine

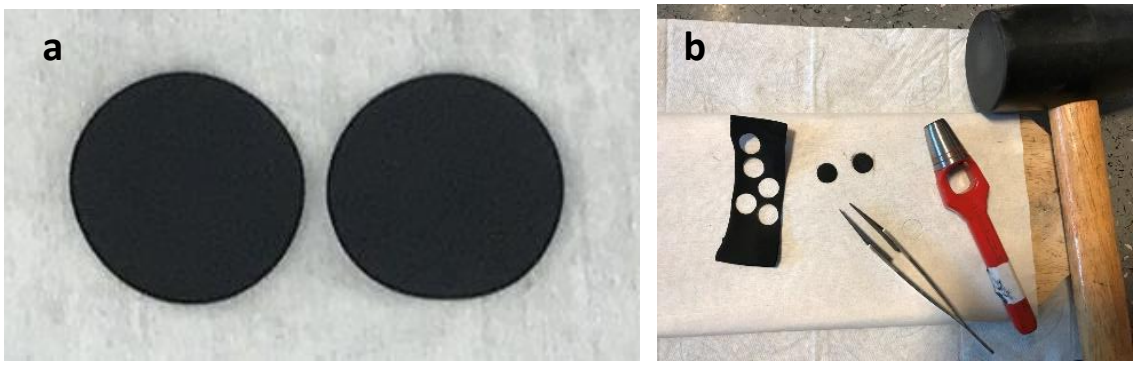

Figure 10. Electrodes preparation:
a. 14 mm electrodes, b. punching with a puncher and a rubber hammer

3.3 Annealing experiment

The electrodes and a smaller square sample used later for sample characterisation are placed in a lab combustion quartz boat. The lab boat is then inserted into the middle off the tube of CVD chamber.

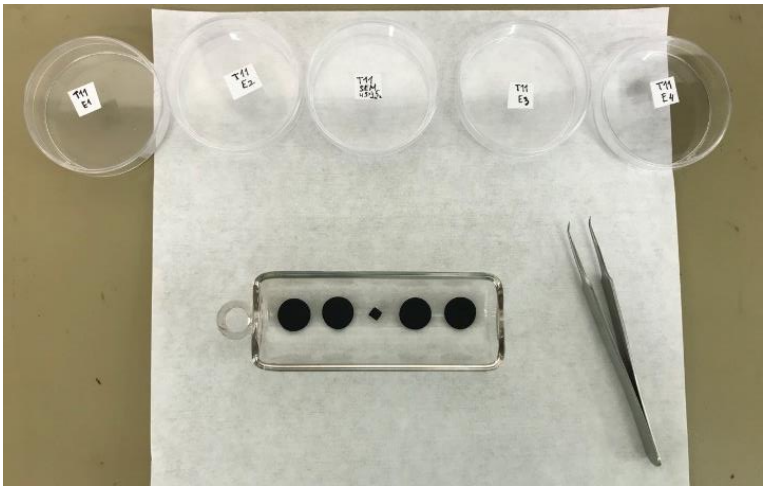

Figure 11. Placing electrodes for in CVD chamber: Electrodes are placed in the combustion quartz boat. Four electrodes are annealed to produce two coin cells per one experiment. A small square piece of a sample is annealed for later sample characterisation

3.4 Coin cell assembly

A coin cell consists of a positive cap, two electrodes separated by a separator, a spacer, a spring and a negative cap. A schematic of coin cell assembly as well as actual parts used for coin cells are shown in Figure 12. The 2032 standard coin cell casing has been used; the ready coin cell assembled is shown in Figure 13.

An exchange of charged particles is facilitated by an electrolyte, in this study tetraethylammonium tetrafluoroborate (TEABF6) has been used as an electrolyte. The volume of 60 uL has been used for one coin cell. To increase a studied voltage window of a capacitor, coin cells are assembled in environment with lower oxygen and humidity level, namely in Glovebox with 0.5 ppm oxygen level and 0.5 ppm humidity level.

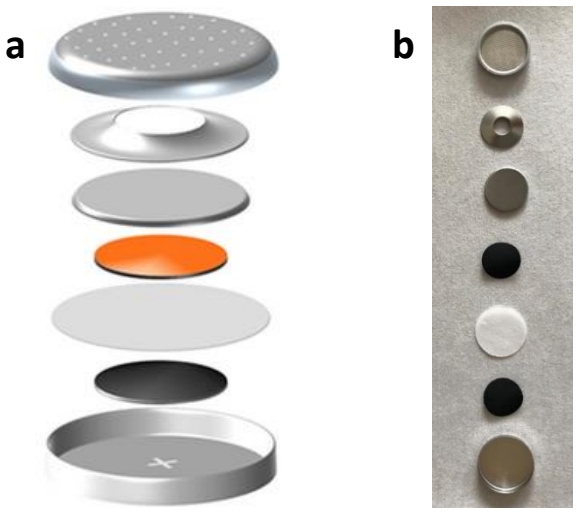

Figure 12. Coin cell assembly: a. A schematic [29]*, b. Actual parts used*

Figure 13. An assembled coin cell

3.5 Measurements and calculations

Assembled coin cells have been tested with Electrochemical Workstation BIO Logic SAS VSP-300 for capacitance, equivalent series resistance (ESR) and self-discharge, which is the main focus of the study. To ensure repeatability of results two coin cells are assembled per experiment. For consistency average values of capacitance, ESR and self-discharge of the two coin cells are considered. Capacitance values of studied coin cells are calculated to be in the range of 20 mF.

3.5.1 Capacitance

The main parameter of supercapacitors is capacitance, which is capability of a device to store electric charge. Capacitance of a coin cell has been measured by running capacitance-voltage test (CV test), where a potential is applied on a coin cell and corresponding current is measured, the result is CV curve, as shown in Graph 2.

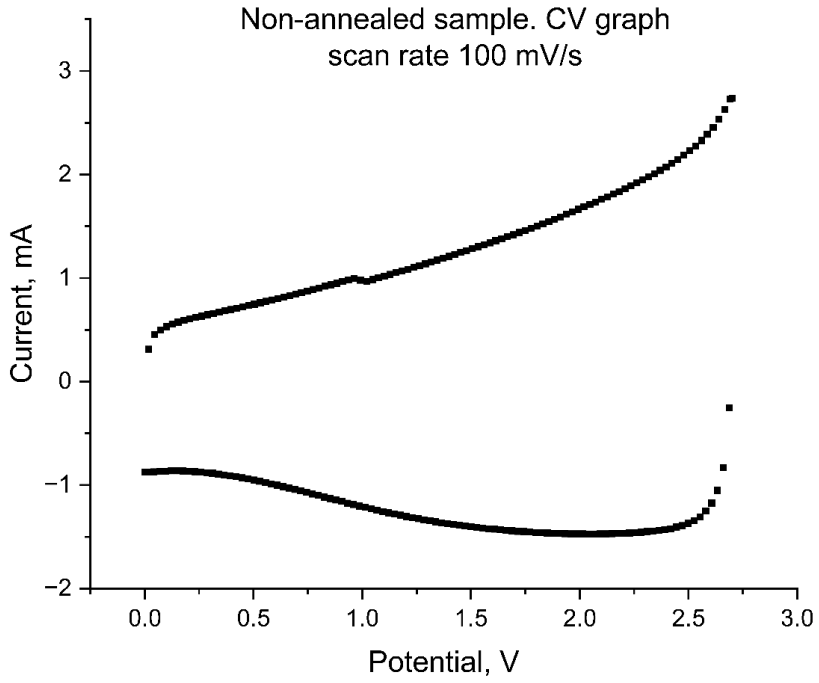

Graph 2. CV curve of non-annealed sample

Areal coin cell capacitance measured in mF/cm^2 is calculated as given in the formula below. The area of the curve has been computed with OriginPro software, area of an

electrode with 14 mm diameter is approximately 1.54 cm^2, CV test is done under 100 mV/s scan rate and voltage window used for testing is 2.7 V.

$$C_{cell\_areal} = \frac{\frac{Area\ of\ the\ curve}{2}}{Area\ of\ an\ electrode * scan\ rate * Voltage\ window} \quad \textit{(Equation 5)}$$

As coin cell capacitance is formed by two electrode capacitances being in series as illustrated in Figure 3, electrodes capacitance is twice as large as coin cell capacitance.

$$C_{electrode} = 2 * C_{cell} \quad \textit{(Equation 6)}$$

So, areal electrode capacitance is calculated as follows.

$$C_{electrode\_areal} = \frac{Area\ of\ the\ curve}{Area\ of\ an\ electrode * scan\ rate * Voltage\ window} \quad \textit{(Equation 7)}$$

Finally, gravimetric electrode capacitance measured in mF/mg, can be found as follows.

$$C_{electrode\_gravimetric} = \frac{Area\ of\ the\ curve}{Area\ of\ an\ electrode * scan\ rate * Voltage\ window} * \frac{1}{CNT\ mass\ per\ area} \quad \textit{(Equation 8)}$$

3.5.2 ESR

To determine equivalent series resistance (ESR) a Nyquist plot is produced, which is a graph of reactance plotted against resistance, measured under varying frequencies. Ra value shown Nyquist plot in Graph 3 corresponds to ESR value of interest. To perform ESR tests, AC current with amplitude of 5 mV and frequency varying from 0.1 Hz to 1 000 000 Hz is applied, corresponding impedance values of a coin cell are recorded as shown in Graph 4.

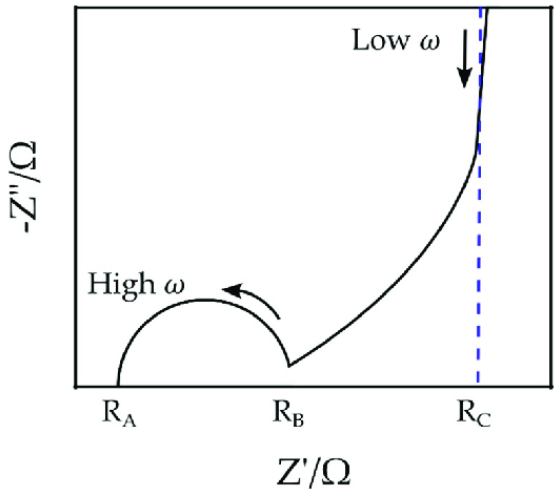

Graph 3. Nyquist plot used to identify ESR. RA value corresponds to ESR [30]

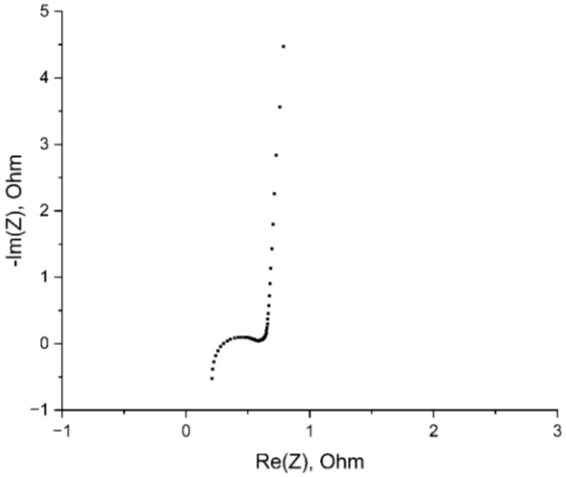

Graph 4. Nyquist plot of a coin cell assembled from non-annealed sample.

3.5.3 Self-discharge

A self-discharge is measured using the electrochemical workstation, which is implemented as follows: a coin cell is charged up to 2.7 V with 5 mA charging current, then 2.7 V level is hold for 2 hours, after that a coin cell is left resting and the open circuit voltage potential of the coin cell is measured. As an example of self-discharge graph, a self-discharge of a coin cell assembled from an annealed sample is shown in Graph 5.

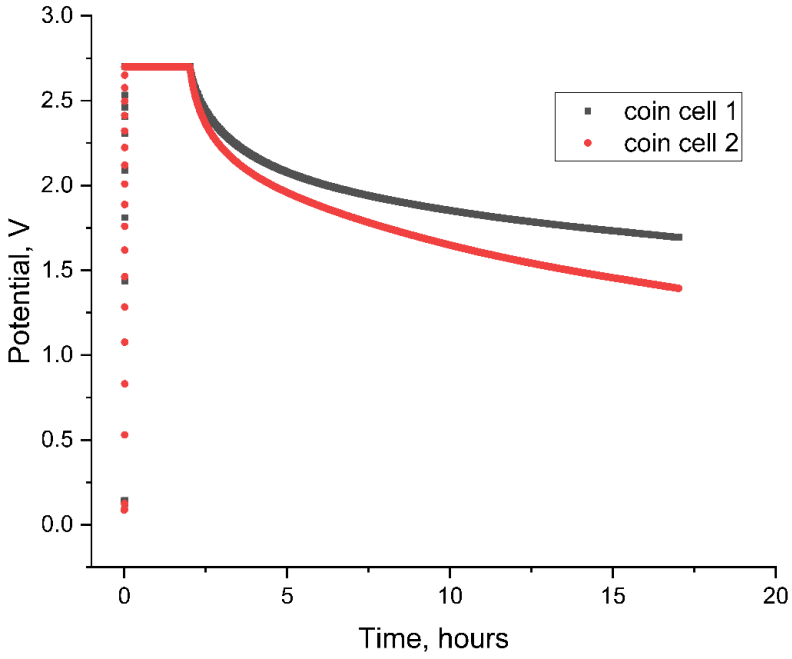

Graph 5. Self-discharge graph of a coin cell assembled from an annealed sample; annealing parameters: 500°C temperature, 30 min duration, H_2:N_2 gas ratio is 40 sccm:200 sccm

4 Results

4.1 Investigation on temperature

For temperature optimisation, experiments have been conducted for same duration of 60 min and H_2:N_2 gas ratio of (50 sccm: 500 sccm), but under different annealing temperatures, varying from 600°C to 200°C, with a step of 100°C. Gravimetric capacitance, ESR and self-discharge results are provided below.

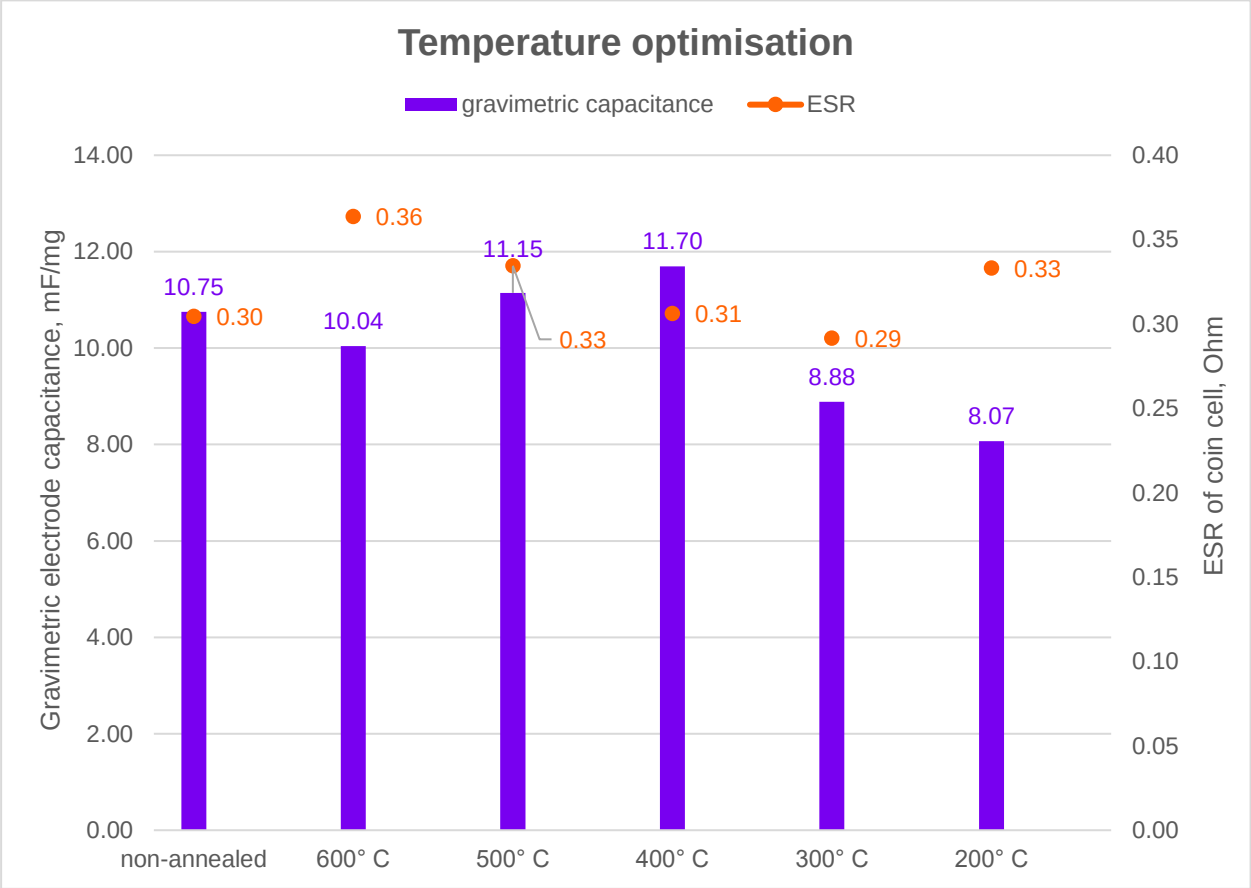

Graph 6. Gravimetric capacitance and ESR as for temperature optimsation. Annealing conditions: 60 minutes duration, 50 sccm : 500 sccm H_2:N_2 gas ratio, temperature has been varied from 600°C to 200°C

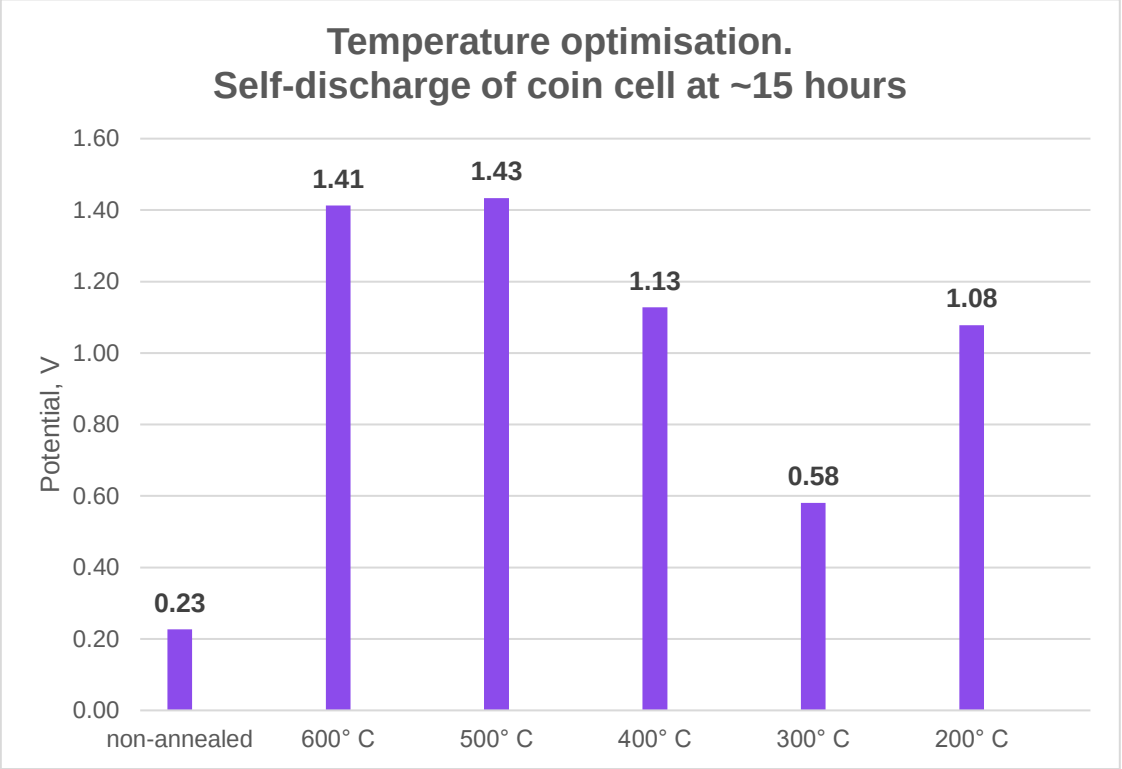

Graph 7. Self-discharge at 60000 s ~ 15 hours. Annealing conditions: 60 minutes duration, 50 sccm : 500 sccm H_2:N_2 gas ratio, temperature has been varied from 600°C to 200°C

It can be seen from Graph 7 that annealing under 500°C gives the best result for self-discharge performance with 1.43 V at 60000 seconds, which is around 15 hours of measurement time. Regarding gravimetric capacitance, as seen from Graph 6 it is on the same level of approximately 10 mF/mg for all temperature values. As for ESR, there is no significant deviation in ESR values with change in annealing temperature.

4.2 Investigation on time

To optimise time, experiments have been conducted for under temperature of 500°C and H_2:N_2 gas ratio of (50 sccm: 500 sccm), but for different annealing duration, varying from 60 minutes to 10 minutes, with a step of 10 minutes. Gravimetric capacitance, ESR and self-discharge results are shown below.

Graph 8. Gravimetric capacitance and ESR as for time optimisation. Annealing conditions: 500°C annealing temperature, 50 sccm : 500 sccm H_2:N_2 gas ratio, annealing temperature varied from 60 min to 10 min

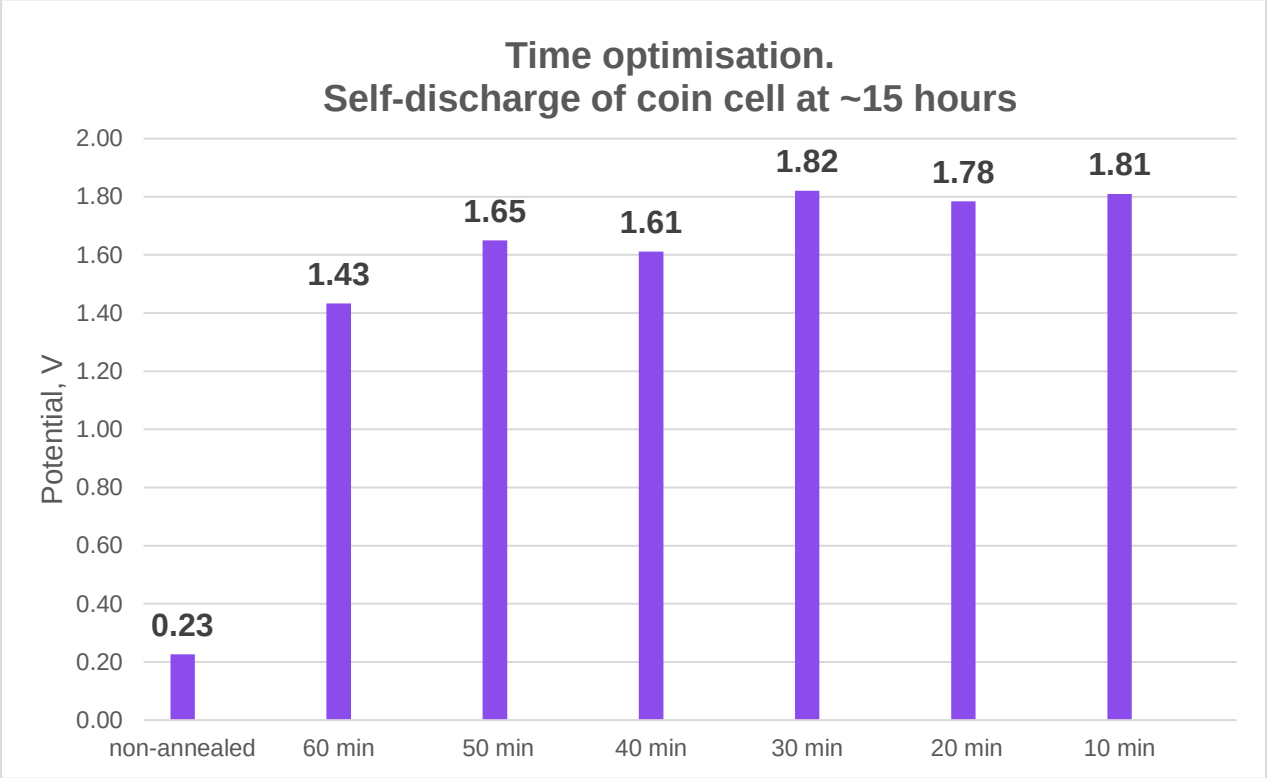

Graph 9. Self-discharge at 60000 s~15 hours for time optimisation.
Annealing conditions: 500°C annealing temperature, 50 sccm : 500 sccm H_2:N_2 gas ratio, annealing temperature varied from 60 min to 10 min

From self-discharge results in Graph 9 it can be observed that 30 minutes of annealing process yields into the best result for self-discharge performance of 1.82 V at 60000 seconds (~ 15 hours) of measurement time. Gravimetric capacitance, as seen from Graph 8 is on determined to be at the level of approximately 11 mF/mg for all durations. There is also no considerable difference in ESR values for varied annealing durations being at a level of 0.30 Ohms.

4.3 Investigation on annealing H_2:N_2 gas composition

For gas flow rate optimisation, experiments have been conducted under temperature of 500°C, for 30 minutes and for such H_2:N_2 gas ratios (in sccm) as 50:500, 100:500, 20:200, 40:200. Gravimetric capacitance, ESR and self-discharge results are given below.

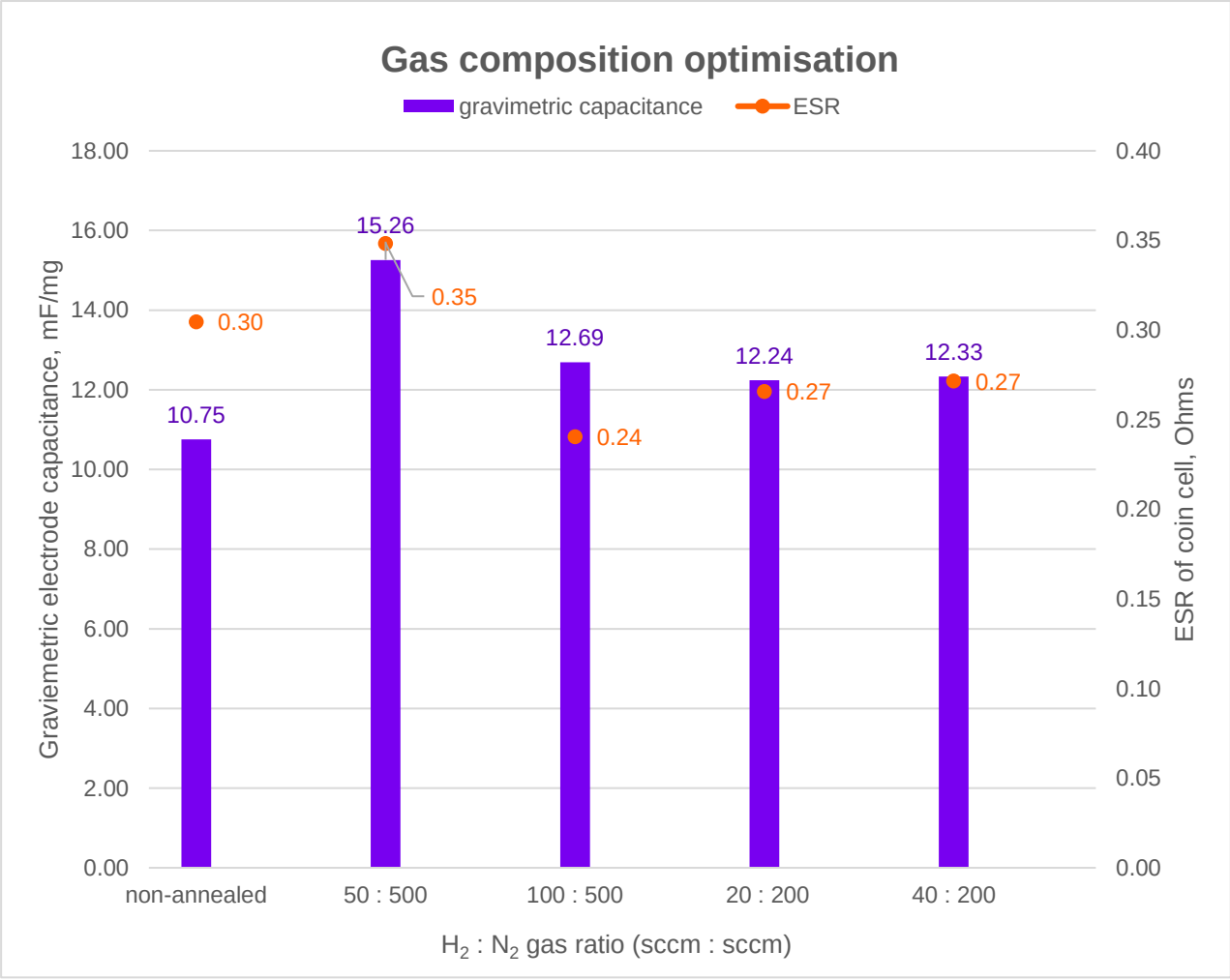

Graph 10. Gravimetric capacitance and ESR results as for H_2:N_2 gas ratio optimisation. Annealing conditions: 500°C annealing temperature, 30 min annealing duration, H_2:N_2 gas ratios tested in sccm: 50 : 500, 100 : 500, 20: 200, 40: 200

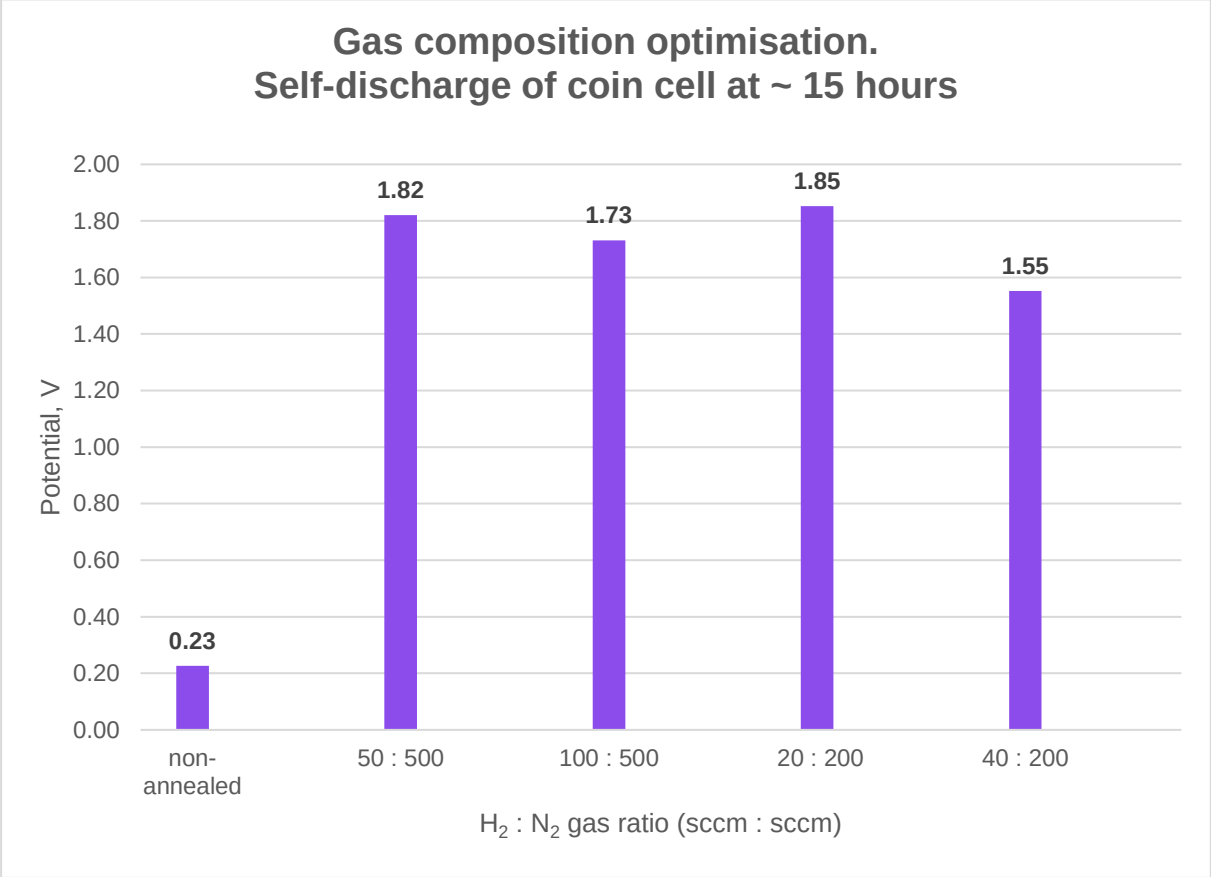

Graph 11. Self-discharge at 60000 s (~15 hours) as for gas ratio optimisation. Annealing conditions: 500°C annealing temperature, 30 min annealing duration, H_2:N_2 gas ratios tested in sccm: 50 : 500, 100 : 500, 20: 200, 40: 200

It can be seen from Graph 11 that hydrogen to nitrogen gas ratio of 20 sccm: 200 sccm provides the best result for self-discharge performance of 1.85 V at 60000 seconds (~ 15 hours) of measurement time. As for gravimetric capacitance, as seen from Graph 10, it takes values of the level of approximately 12 mF/mg for all considered gas ratios. With regards to ESR, it shows consistent behaviour being at a level of 0.30 Ohms.

From optimisation of annealing temperature, annealing duration and H_2:N_2 gas ratio, it can be deducted that the optimal recipe for self-discharge improvement is 500°C temperature, 30 minutes duration and 20 sccm:200 sccm hydrogen to nitrogen ratio.

4.4 Comparison of non-annealed and annealed electrodes performance

To analyse a difference between self-discharge performance of supercapacitors assembled from non-annealed electrodes and annealed electrodes, a self-discharge graph is provided below. For annealing parameters an optimal recipe has been used, which is 500°C temperature, 30 minutes duration and 20 sccm:200 sccm H_2:N_2 gas composition.

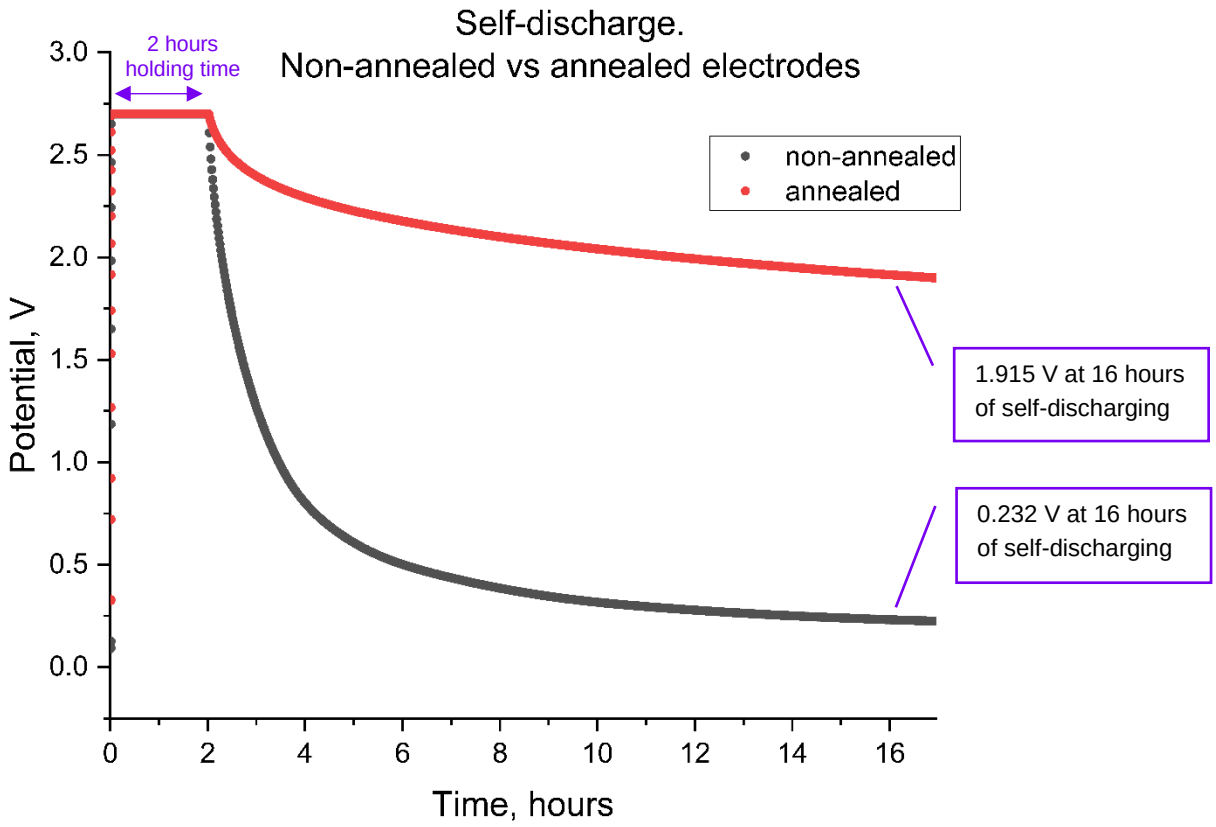

Graph 12. Self-discharge plot of supercapacitors with non-annealed and annealed electrodes. Annealing parameters are 500°C temperature, 30 minutes duration and 20 sccm:200 sccm H_2:N_2 gas composition.

After conducting self-discharge tests, it has been determined that coin cells assembled from non-electrodes had 0.232 V after 16 hours of self-discharging, with 2.468 V being lost as compared to initial charge of 2.7V. This means 91.4 % of the initial charge has been lost by using regular non-annealed electrodes.

In comparison, coin cells assembled from annealed electrodes had 1.915 V after 16 hours of self-discharging, with 0.785 V being lost as compared to initial charge of 2.7V. This means only 29.1 % of the initial has been lost by using annealed electrodes. Thus, annealing using optimal recipe conditions can yield in 62.3 % improvement of self-discharge performance.

4.5 Comparison of annealed electrodes-based coin cell with commercial cell

To understand how studied annealed electrodes are compared with current commercial solutions, self-discharge tests have been applied to a coin cell assembled from annealed electrodes and a commercial cell. A commercial capacitor ELN of 220 mF and 3.3 V voltage window has been considered, as it was a capacitor that was of the same type (single cell) and mostly close with capacitance and voltage window values among those available in the laboratory. For annealing parameters an optimal recipe has been used, which is 500°C temperature, 30 minutes duration and 20 sccm:200 sccm H_2:N_2 gas composition.

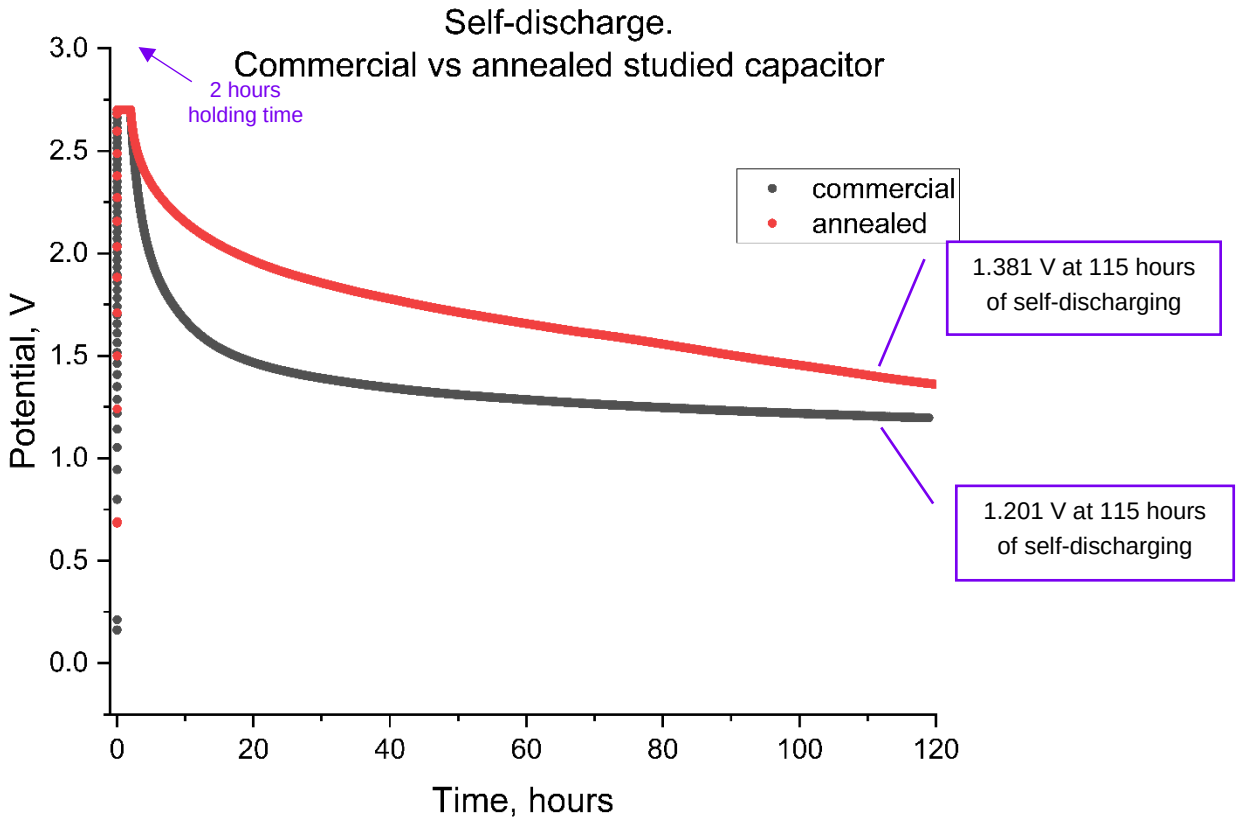

Graph 13. Self-discharge plots of a commercial capacitor and a capacitor assembled from annealed electrodes. Annealing parameters are 500°C temperature, 30 minutes duration and 20 sccm:200 sccm H_2:N_2 gas composition.

Having conducted long self-discharge tests for 117 hours, which is around 5 days of measurement, it has been observed that a commercial cell had 1.201 V at 115 hours of self-discharging, with 1.499 V being lost as compared to initial charge of 2.7 V. This means 55.5 % of the initial charge has been lost for the commercial capacitor.

As for a capacitor assembled from annealed electrodes, it had 1.381 V after 115 hours of self-discharging, with 1.319 V being lost as compared to initial charge of 2.7V. This means 48.9 % of the initial charge has been lost for the studied annealed electrodes-based capacitor. Thus, annealing using optimal recipe conditions demonstrates 6.6 % better self-discharge performance in long term in comparison to the commercial capacitor.

What is more, the studied annealed electrode-based capacitor has around 20 mF capacitance, compared to 220 mF capacitance of the commercial capacitance. Moreover, capacitors with higher capacitance can charge to larger electric charge, thus having lower self-discharge rate, meaning the larger capacitance is, the better is self-discharge performance. Therefore, had the studied annealed electrodes-based capacitor be of larger capacitance close to 220 mF, it would show even better performance. This shows the considerable improvement of self-discharge performance with proposed annealing method.

5 Discussion

5.1 Sample characterisation

Sample charactersiation techniques of non-annealed sample and a sample annealed under optimal annealing recipe have been performed to understand how the annealing affect the samples. Such characterisation techniques as field-emmision scanning electron microscopy (FE-SEM), energy dispersive spectroscopy (EDX) and X-ray diffraction (XRD) have been implemented.

5.1.1 FE-SEM characterisation

To analyse morphology of CNTs, the sample surface has been analysed using field-emission scanning electron microscope (FE-SEM). From the FE-SEM image it can observed that morphology of a sample did not change after annealing. In 200K magnified FE-SEM images of non-annealed and annealed samples, a multi-layered shell-like structure of CNT can be noticed. It can be explained by the multi-walled structure of CNTs synthesised with CVD process.

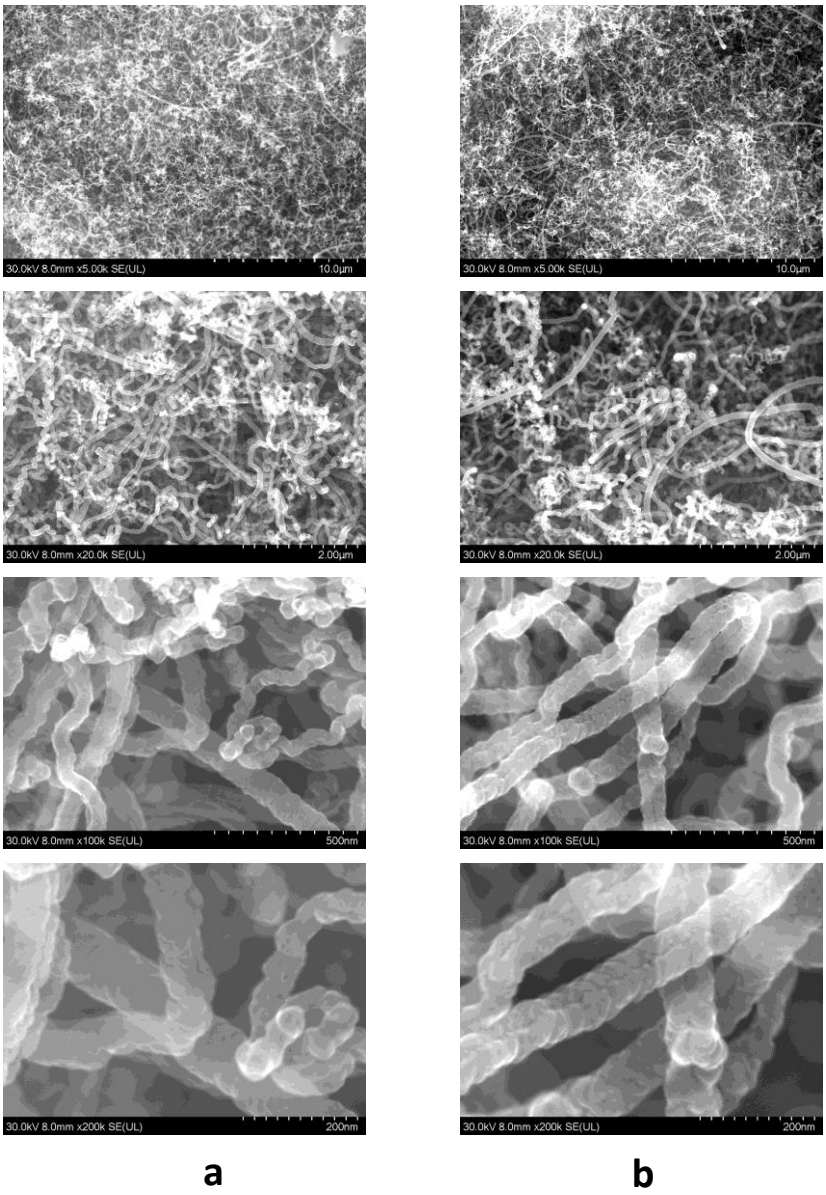

Figure 14. FE-SEM image of CNTs under 5K, 20K, 100K and 200K magnification: a. non-annealed sample, b. annealed sample

5.1.2 EDX characterisation

Energy dispersive X-ray spectroscopy (EDX) has been performed to make elemental analysis of non-annealed and annealed samples.

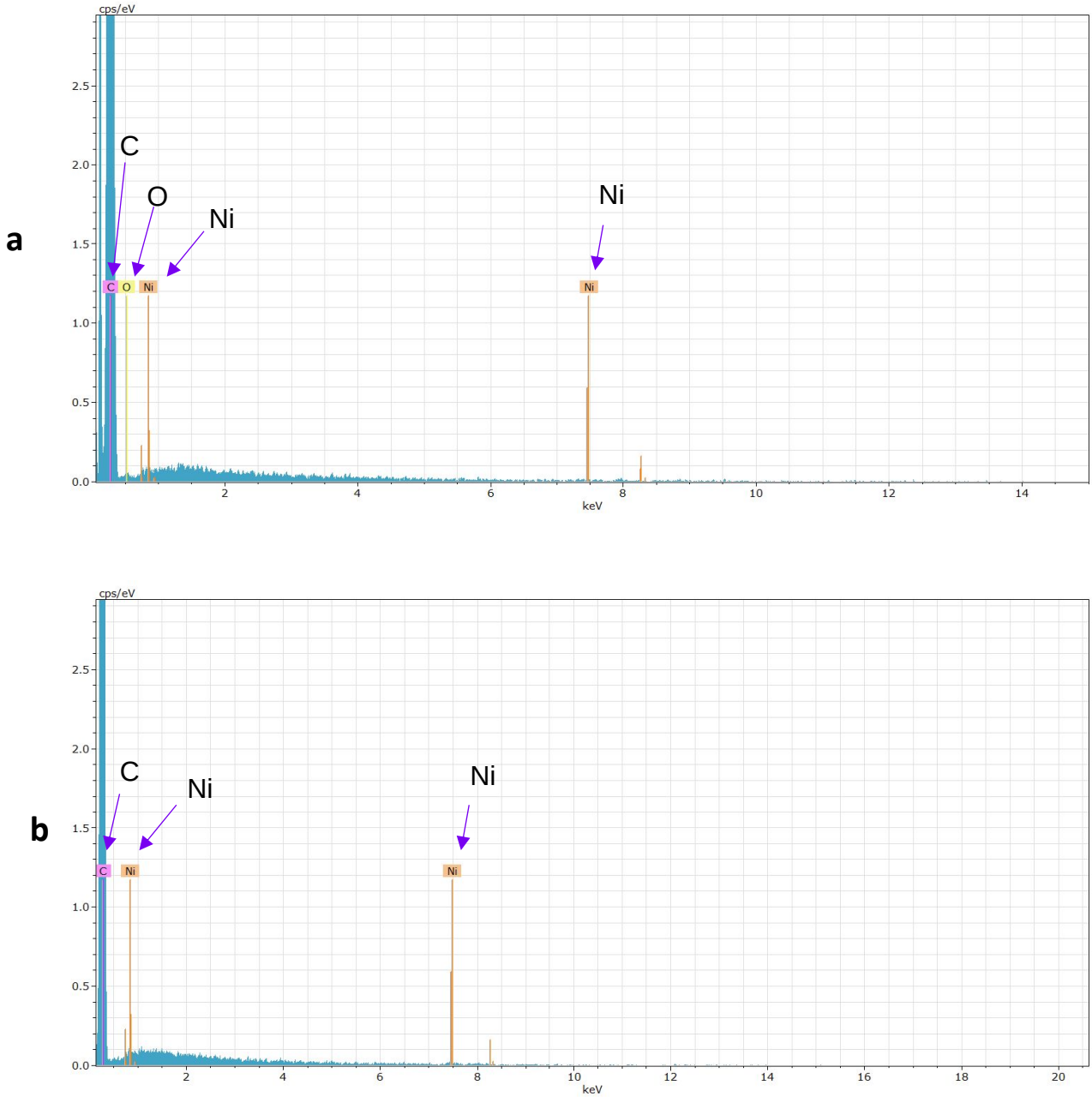

Figure 15. EDX spectrum: a. non-annealed sample, b. annealed sample

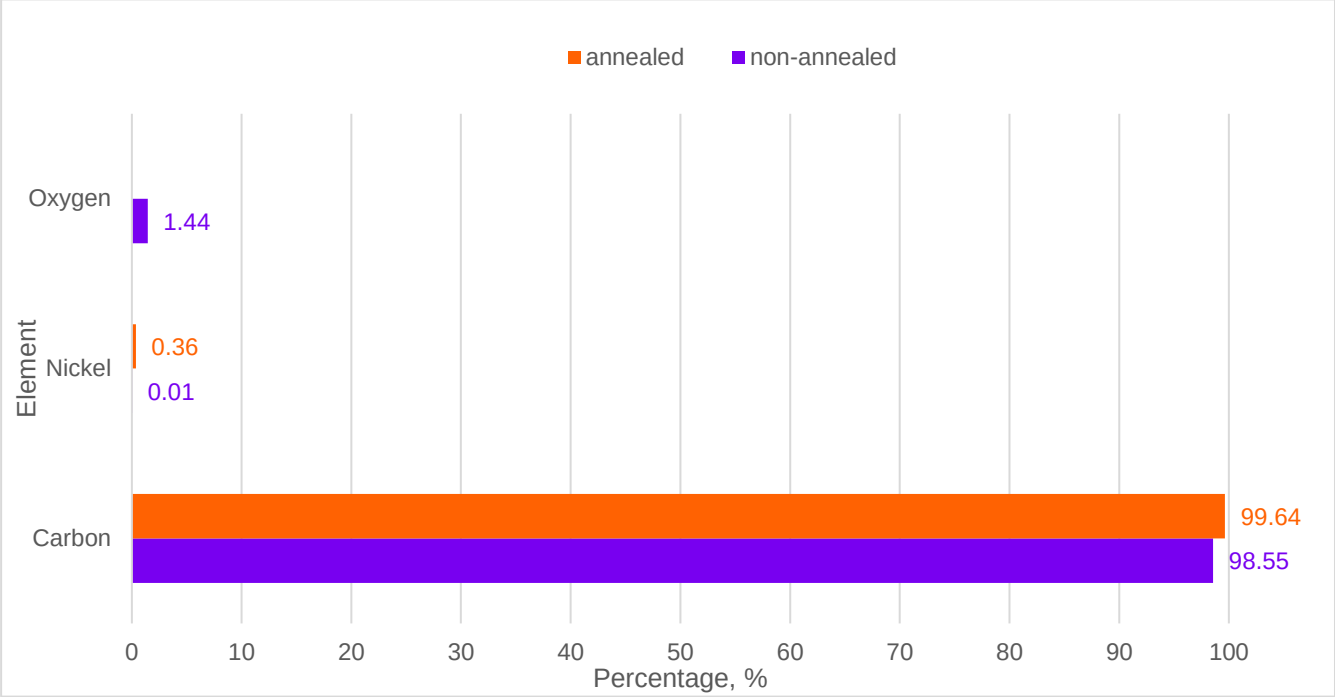

Graph 14. Elemental composition of a sample

From EDX characterisation results shown in Figure 15 and Graph 14 it can be seen that before annealing CNTs consist mostly of carbon (98.55 %), oxygen (1.44 %) and nickel (0.01 %).

The oxygen contamination can be explained by the presence of functional groups on the surface of CNT electrodes produced during CNT synthesis process as a result of a reaction of oxygen from $NiSO_4$ with carbon. The content of nickel shows the presence of nickel nanoparticles on CNT electrode surface.

It can be observed that after annealing oxygen has been removed from the CNTs completely. One can notice a higher percentage of nickel of annealed sample, this can be due to limited accuracy of EDX technique.

5.1.3 XRD characterisation

X-ray diffraction (XRD) characterisation have been performed to identify crystalline structure of non-annealed and annealed samples.

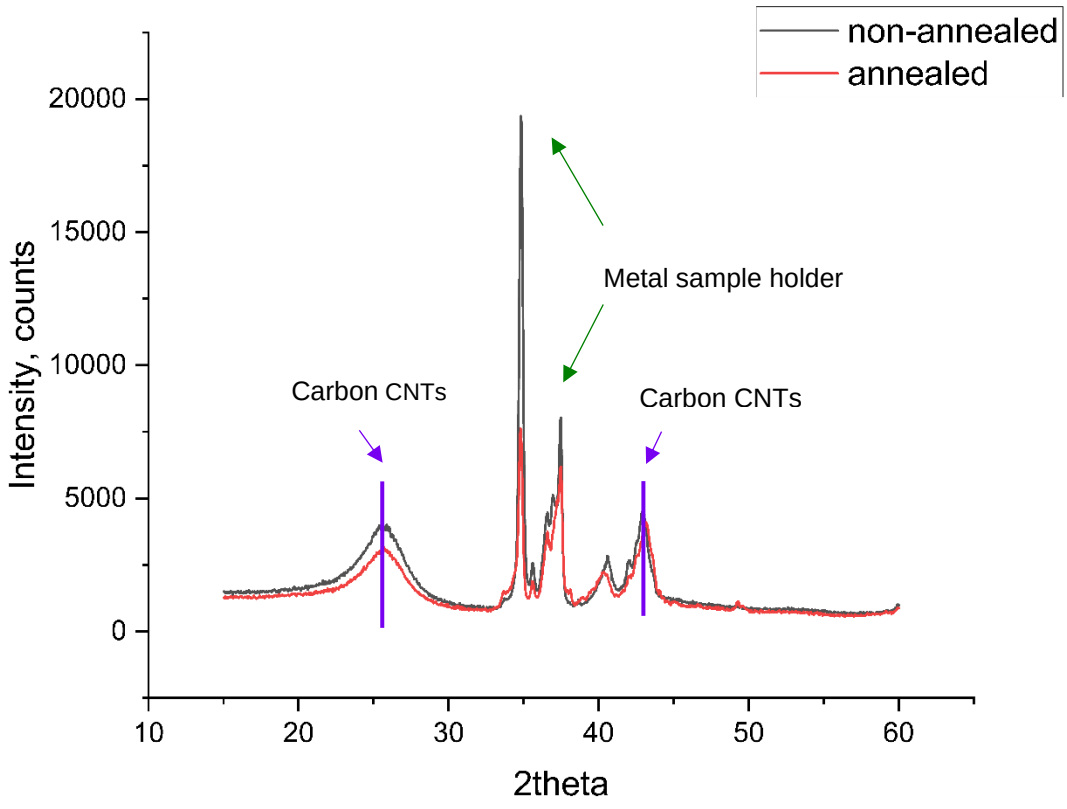

Figure 16. XRD characterisation of non-annealed and annealed sample

As can be seen from Figure 16, the peaks that correspond to diffraction pattern of carbon CNTs [31] are not altered in terms of shape and sharpness. This means that the proposed annealing treatment does not affect structure of CNTs, implying that capacitance properties of supercapacitors are not likely to be affected by the annealing.

5.2 Limitations

Considering limitations, it is necessary to note that the number of experiments has been limited due to time and sample quantity constraints.

Namely, for temperature optimisation values from 600°C to 200°C has been considered with a step difference of 100°C. For the future work a smaller step difference of 50°C can be considered, and in the vicinity of optimal temperature of 500°C a step difference of 10°C can be implemented.

Similarly, for time optimisation periods of 60 min to 10 min have been implemented with a step difference of 10 min. For future considerations, a smaller step difference of 5 min can be considered, and in the vicinity of optimal time 30 minutes a step difference of 1 min can be taken into account.

Furthermore, for hydrogen and nitrogen gas composition optimisation, such H_2:N_2 gas flow ratios as 50 sccm : 500 sscm, 100 sccm : 500 sscm, 20 sccm : 200 sscm and 40 sccm : 200 sscm have been considered. The reason for this is to understand the main pattern of gas flows influence on self-discharge. For the future, more extensive range of ratios close to the optimal one can be considered, e.g. including such ratios as 10 sccm : 200 sscm, 15 sccm : 200 sscm, 25 sccm : 200 sscm and 30 sccm : 200 sscm.

5.3 Challenges

One of the main challenges of the project was to perform XRD sample characterisation because there was a strong signal from aluminium substrate distorting XRD diffraction pattern of CNT samples. To overcome this issue, CNTs was scrubbed out the sample substrate, and XRD characterisation has been applied only CNTs powder. There was still a signal from metallic sample holder, but it did not have major distortion affect. In the future work, glass sample holder can be used to record only XRD signals of carbon material.

Another challenge was to maintain stable oxygen level at 0.5 ppm level in Glovebox during coin cell assembly. It was observed that higher contamination of oxygen negatively affected self-discharge performance as well as gravimetric capacitance of samples. To avoid negative influence of oxygen contamination during coin cell assembly, the oxygen level was closely monitored before during and after coin cell assembly. Moreover, Glovebox was carefully maintained, including periodic regeneration, cleaning and filter change.

5.4 Future considerations

Considering future improvements, leakage current tests of assembled coin cells can be implemented in addition to capacitance, ESR and self-discharge parameters. This might help to have a broader picture of self-discharge performance and its relation to annealing parameters.

Furthermore, different types of casing can be implemented during a stage of coin cell assembly. To be more precise, gold plated positive and negative caps can be considered in the future for supercapacitor casings. Being high-conductive, golden plated casing can improve ESR as well self-discharge performance even further in addition to hydrogen and nitrogen annealing.

In addition, more material characterization could be done in the future work, such as X-ray photoelectron spectroscopy (XPS) and high accuracy Fourier Transform Infrared Spectroscopy (FTIR) to fully disclose the underlying mechanism of lowering the self-discharge from the perspective of material research. To be more precise, XPS characterisation can be applied to do elemental analysis of a sample, which can be much more accurate that EDX applied in current study. As for FTIR, it can provide information on presence and types of functional groups on the surface of electrodes.

6 Conclusions

After numerous experiments and tests, an optimal recipe of hydrogen and nitrogen annealing of CNT samples for improved self-discharge performance of CNT based supercapacitors has been produced. Namely, the annealing needs to be performed under 500°C temperature, for 30 minutes and with 20 sccm:200 sccm H_2:N_2 gas composition

Implementing the optimal recipe, a significant decrease in self-discharge has been achieved from the loss of 91.4% to 29.1% of initial 2.7 V charge for supercapacitors of 20 mF capacitance, resulting in 62.3% of improvement.

Comparing to a commercial capacitor, the studied supercapacitors made of electrodes annealed under optimal recipe conditions showed 6.6% better self-discharge performance.

From careful sample characterisation, it has been studied that the annealing does not affect the morphology and crystalline structure of CNT samples. Thus, significant suppress of self-discharge has been achieved without affecting CNT structure and capacitance of supercapacitors. Improvement of self-discharge can be due to reduction of functional group concentration, resulting in decrease of oxygen contamination in CNTs and purifying of CNT surface of electrodes.

To improve self-discharge performance further, closer consideration of annealing parameters, usage of gold-plated coin cell cases as well as advanced sample characterisation techniques for detailed study of samples can be considered for future work.

References

[1] V. Popov, “Carbon nanotubes: properties and application,” *Materials Science and Engineering: R: Reports*, vol. 43, no. 3, pp. 61–102, Jan. 2004, doi: 10.1016/j.mser.2003.10.001.

[2] F. Daneshvar, H. Chen, K. Noh, and H.-J. Sue, “Critical challenges and advances in the carbon nanotube–metal interface for next-generation electronics,” *Nanoscale Adv*, vol. 3, no. 4, pp. 942–962, 2021, doi: 10.1039/D0NA00822B.

[3] H. Dai, “Carbon nanotubes: opportunities and challenges,” *Surf Sci*, vol. 500, no. 1–3, pp. 218–241, Mar. 2002, doi: 10.1016/S0039-6028(01)01558-8.

[4] M. Filchakova and V. Saik, “Single-walled carbon nanotubes: structure, properties, applications, and health & safety,” https://tuball.com/articles/single-walled-carbon-nanotubes.

[5] Q. Zhang, J. Rong, and B. Wei, “A divided potential driving self-discharge process for single-walled carbon nanotube based supercapacitors,” *RSC Adv*, vol. 1, no. 6, p. 989, 2011, doi: 10.1039/c1ra00318f.

[6] E. Frackowiak and F. Béguin, “Carbon materials for the electrochemical storage of energy in capacitors,” *Carbon N Y*, vol. 39, no. 6, pp. 937–950, May 2001, doi: 10.1016/S0008-6223(00)00183-4.

[7] P. Simon and Y. Gogotsi, “Materials for electrochemical capacitors,” *Nat Mater*, vol. 7, no. 11, pp. 845–854, Nov. 2008, doi: 10.1038/nmat2297.

[8] M. F. L. De Volder, S. H. Tawfick, R. H. Baughman, and A. J. Hart, “Carbon Nanotubes: Present and Future Commercial Applications,” *Science (1979)*, vol. 339, no. 6119, pp. 535–539, Feb. 2013, doi: 10.1126/science.1222453.

[9] M. L. Terranova, V. Sessa, and M. Rossi, “The World of Carbon Nanotubes: An Overview of CVD Growth Methodologies,” *Chemical Vapor Deposition*, vol. 12, no. 6, pp. 315–325, Jun. 2006, doi: 10.1002/cvde.200600030.

[10] O. Zaytseva and G. Neumann, “Carbon nanomaterials: production, impact on plant development, agricultural and environmental applications,” *Chemical and Biological Technologies in Agriculture*, vol. 3, no. 1, p. 17, Dec. 2016, doi: 10.1186/s40538-016-0070-8.

[11] K. S. Ibrahim, “Carbon nanotubes-properties and applications: a review,” *Carbon letters*, vol. 14, no. 3, pp. 131–144, Jul. 2013, doi: 10.5714/CL.2013.14.3.131.

[12] H. Dai, “Carbon Nanotubes: Synthesis, Integration, and Properties,” *Acc Chem Res*, vol. 35, no. 12, pp. 1035–1044, Dec. 2002, doi: 10.1021/ar0101640.

[13] J. M. Schnorr and T. M. Swager, “Emerging Applications of Carbon Nanotubes,” *Chemistry of Materials*, vol. 23, no. 3, pp. 646–657, Feb. 2011, doi: 10.1021/cm102406h.

[14] P. M. Ajayan and O. Z. Zhou, “Applications of carbon nanotubes,” *Carbon nanotubes: synthesis, structure, properties, and applications*, pp. 391–425, 2001.

[15] H. Pan, J. Li, and Y. P. Feng, “Carbon Nanotubes for Supercapacitor,” *Nanoscale Res Lett*, vol. 5, no. 3, pp. 654–668, Mar. 2010, doi: 10.1007/s11671-009-9508-2.

[16] E. Frackowiak, K. Metenier, V. Bertagna, and F. Beguin, “Supercapacitor electrodes from multiwalled carbon nanotubes,” *Appl Phys Lett*, vol. 77, no. 15, pp. 2421–2423, Oct. 2000, doi: 10.1063/1.1290146.

[17] R. Vicentini *et al.*, “Multi-walled carbon nanotubes and activated carbon composite material as electrodes for electrochemical capacitors,” *J Energy Storage*, vol. 33, p. 100738, Jan. 2021, doi: 10.1016/j.est.2019.04.012.

[18] P. Svasta, R. Negroiu, and Al. Vasile, “Supercapacitors — An alternative electrical energy storage device,” in *2017 5th International Symposium on Electrical and Electronics Engineering (ISEEE)*, IEEE, Oct. 2017, pp. 1–5. doi: 10.1109/ISEEE.2017.8170626.

[19] W. Shang *et al.*, “Insight into the self-discharge suppression of electrochemical capacitors: Progress and challenges,” *Advanced Powder Materials*, vol. 2, no. 1, p. 100075, Jan. 2023, doi: 10.1016/j.apmate.2022.100075.

[20] R. Yuan, Y. Dong, R. Hou, S. Zhang, and H. Song, “Review—Influencing Factors and Suppressing Strategies of the Self-Discharge for Carbon Electrode Materials in Supercapacitors,” *J Electrochem Soc*, vol. 169, no. 3, p. 030504, Mar. 2022, doi: 10.1149/1945-7111/ac56a1.

[21] V. V. N. Obreja, “On the performance of supercapacitors with electrodes based on carbon nanotubes and carbon activated material—A review,” *Physica E Low Dimens Syst Nanostruct*, vol. 40, no. 7, pp. 2596–2605, May 2008, doi: 10.1016/j.physe.2007.09.044.

[22] M. M. Ovhal, N. Kumar, S.-K. Hong, H.-W. Lee, and J.-W. Kang, “Asymmetric supercapacitor featuring carbon nanotubes and nickel hydroxide grown on carbon fabric: A study of self-discharging characteristics,” *J Alloys Compd*, vol. 828, p. 154447, Jul. 2020, doi: 10.1016/j.jallcom.2020.154447.

[23] C. Hao, X. Wang, Y. Yin, and Z. You, “Analysis of Charge Redistribution During Self-discharge of Double-Layer Supercapacitors,” *J Electron Mater*, vol. 45, no. 4, pp. 2160–2171, Apr. 2016, doi: 10.1007/s11664-016-4357-0.

[24] W. Zhang *et al.*, “Self-discharge of supercapacitors based on carbon nanotubes with different diameters,” *Electrochim Acta*, vol. 357, p. 136855, Oct. 2020, doi: 10.1016/j.electacta.2020.136855.

[25] Q. Zhang, C. Cai, J. Qin, and B. Wei, “Tunable self-discharge process of carbon nanotube based supercapacitors,” *Nano Energy*, vol. 4, pp. 14–22, Mar. 2014, doi: 10.1016/j.nanoen.2013.12.005.

[26] S.-C. Wang, J. Yang, X.-Y. Zhou, and J. Xie, “The contribution of functional groups in carbon nanotube electrodes to the electrochemical performance,” *Electronic Materials Letters*, vol. 10, no. 1, pp. 241–245, Jan. 2014, doi: 10.1007/s13391-013-3116-0.

[27] C. Qiu, L. Jiang, Y. Gao, and L. Sheng, “Effects of oxygen-containing functional groups on carbon materials in supercapacitors: A review,” *Mater Des*, vol. 230, p. 111952, Jun. 2023, doi: 10.1016/j.matdes.2023.111952.

[28] K. Liu *et al.*, “Recent research advances of self-discharge in supercapacitors: Mechanisms and suppressing strategies,” *Journal of Energy Chemistry*, vol. 58, pp. 94–109, Jul. 2021, doi: 10.1016/j.jechem.2020.09.041.

[29] Z. Xue *et al.*, “Research on the assembly process of full coin cells: key factors affecting data reliability,” *Ionics (Kiel)*, vol. 29, no. 12, pp. 5285–5293, Dec. 2023, doi: 10.1007/s11581-023-05225-2.

[30] D. Peyrow Hedayati, G. Singh, M. Kucher, T. D. Keene, and R. Böhm, “Physicochemical Modeling of Electrochemical Impedance in Solid-State Supercapacitors,” *Materials*, vol. 16, no. 3, p. 1232, Jan. 2023, doi: 10.3390/ma16031232.

[31] S. H, “Synthesis of Carbon Nanotubes for Oil-water Interfacial Tension Reduction,” *Oil & Gas Research*, vol. 1, no. 1, 2015, doi: 10.4172/2472-0518.1000104.

List of tables, graphs and figures

Annex: Equipment used

CVD tube furnaced used for annealing

.

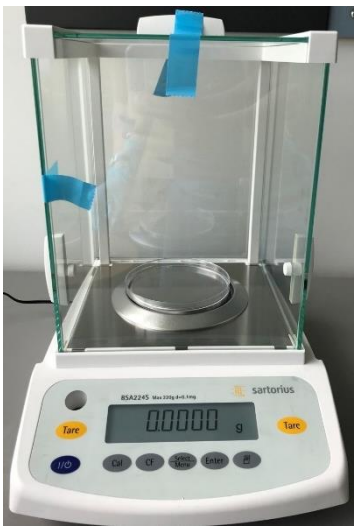

Weighing scale

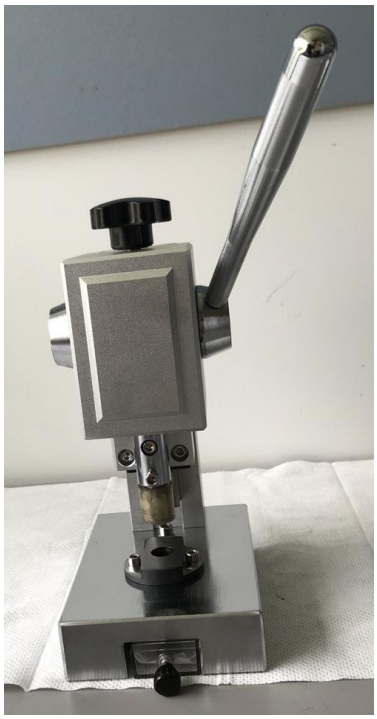

Punching machine used to punch out electrodes from a strip sample

Pressing machine used to straighten curved electrodes

Glovebox
MBraun Easylab

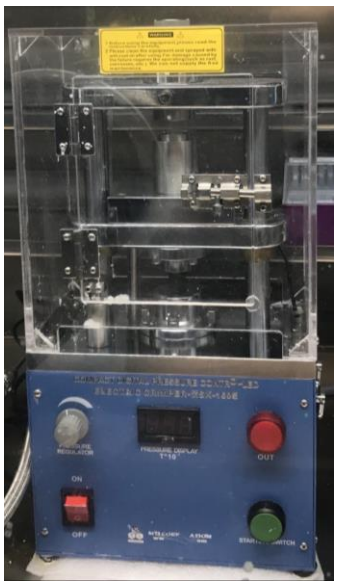

Compact Digital Pressure Controlled
Electric Crimping/De-Crimping Machine

Electrochemical Workstation
BIO Logic SAS

Testing channel of electrochemical workstation

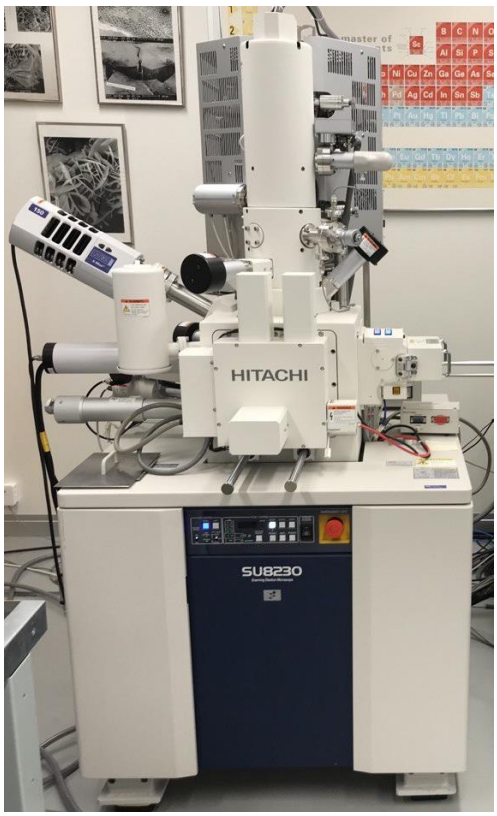

Field emission scanning electron microscope (FE-SEM)

Scanning electron microscope (SEM) Hitachi SU 3500

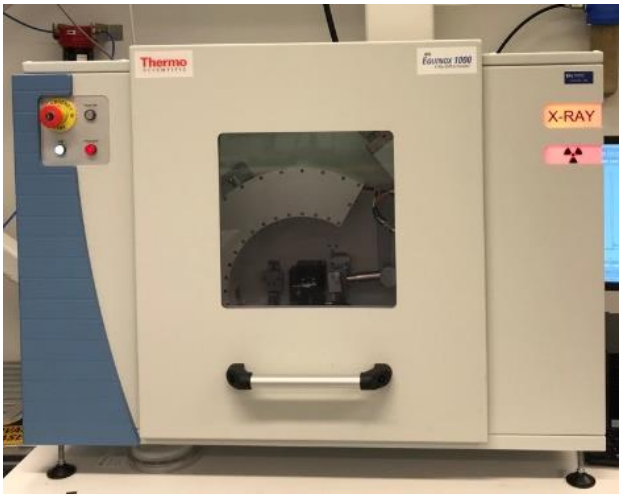

X-Ray Diffractometer (XRD) Inel Equinox 1000

Some of assembled coin cells